Accepted Manuscript

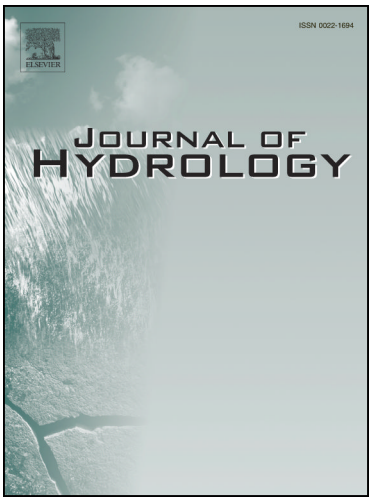

Research papers

Optimization of the hydrodynamic characteristics of a karst conduit with CFPv2 coupled to OSTRICH

Zargham Mohammadi, Walter A. Illman, Masoud Karimi

PII: S0022-1694(18)30819-9
DOI: https://doi.org/10.1016/j.jhydrol.2018.10.050
Reference: HYDROL 23214

To appear in: *Journal of Hydrology*

Received Date: 1 April 2018
Revised Date: 17 October 2018
Accepted Date: 20 October 2018

Please cite this article as: Mohammadi, Z., Illman, W.A., Karimi, M., Optimization of the hydrodynamic characteristics of a karst conduit with CFPv2 coupled to OSTRICH, *Journal of Hydrology* (2018), doi: https://doi.org/10.1016/j.jhydrol.2018.10.050

Optimization of the hydrodynamic characteristics of a karst conduit with CFPv2 coupled to OSTRICH

Zargham Mohammadi[a,b,*], Walter A. Illman[b], Masoud Karimi[a]

[a] Department of Earth Sciences, Faculty of Sciences, 7146713565, Shiraz University, Shiraz, Iran.

[b] Department of Earth and Environmental Sciences, 200 University Ave. W, Waterloo, Ontario, N2L 3G1, Canada

[*] Corresponding author: z.mohammadi@uwaterloo.ca

Key words: karst groundwater modeling; CFPv2; OSTRICH; MODFLOW-CFP; optimization; dye tracing; Iran

Abstract

In order to better define the characteristics of a karst conduit, an integrated hydrogeological study including numerical modeling using CFPv2 is conducted at a karst aquifer in the Zagros Mountain Region of Iran. The Sarvak limestone aquifer in the Nil Anticline is the main karst aquifer of the study area with major groundwater discharge taking place at Sarkur spring. An annual water balance and a dye tracing test confirmed that the karst system is mainly recharged through rainfall and the Maroon River. Several depressions are observed along the banks of the river with a major one classified as a sinkhole used for dye injection. A groundwater flow model was developed based on the available hydrogeological information. A probable direct conduit flow path with an estimated groundwater flow velocity of 96 m/h is estimated between the injection point and the Sarkur spring. Four scenarios are assumed to simulate the probable conduit flow path using the CFPv2 code. As one of the first attempts in regional groundwater flow modeling of a karst aquifer, CFPv2 is automatically calibrated with field measurements of spring discharge and a dye breakthrough curve through a parameter estimation code OSTRICH to optimize the characteristics of the conduit through the minimization of the weighted sum of square error. Simulated results reveal that a conduit with a diameter of 2.9 m is required to adequately simulate spring discharge and dye tracer migration between the injection and discharge points. Our new approach (linking of CFPv2 and OSTRICH) provides a deeper understanding of groundwater flow and solute transport in karst terrains even when available data are limited and the approach should be applicable to other areas.

Key words: karst groundwater modeling; CFPv2; OSTRICH; MODFLOW-CFP; optimization; dye tracing; Iran

1. Introduction

It is estimated that more than 25% of the world population directly utilizes karst water resources for drinking water purposes (Ford and Williams, 2013). However, karst terrains are inherently heterogeneous and complex. Generally, a wide range of porosity including micro-fracture porosity to large conduit and caves are active in a well-developed karst aquifer. As a consequence, several well-known methods have been introduced in the literature to study karst and to overcome its complexity (Ford and Williams, 2013; Goldscheider and Drew, 2007). Given the heterogeneity of karst rocks, an integrated study is necessary.

Investigation of karst terrains should be followed by a step-by-step strategy using different approaches at local and regional scales (Bakalowicz, 2005; Mohammadi et al., 2007a). These approaches start from basic field hydrogeological studies and culminate in the mathematical modeling of groundwater flow and mass transport. Valuable information is obtained from the general methodology of karst study (Bakalowicz, 2005; Goldscheider and Drew, 2007) including 1) geological, geomorphological, and speleological investigations, 2) water balance studies, 3) spring hydrograph and time series analysis, 4) hydrochemical and isotopic methods (i.e., natural tracing), 5) artificial tracing, 6) analysis of ambient spatial and temporal variations of piezometer data, and 7) pumping tests. Although an integrated and comprehensive study requires the implementation of all these methods, dye tracer tests are specifically used to determine the hydraulic connections of karst features in a heterogeneous

karst terrain (Borghi et al., 2016; Mohammadi et al., 2007b; Morales-Juberías et al., 1997; Mozafari et al., 2012; Smart and Ford, 1986). In order to obtain data for water movement and conveyance of pollutants for all hydrological and hydrogeological studies, dye tracer test is a well-known method (Kass and Behrens, 1998). Generally, a combination of all structural, hydrochemical, isotopic and hydraulic data obtained from a karst aquifer are used to construct a conceptual model that is translated to a mathematical model.

Given the heterogeneity of karst aquifers, different types of mathematical models have been developed in the literature. Four major approaches include: 1) equivalent porous media (Scanlon et al., 2003; Teutsch, 1990); 2) discrete fracture or conduit network (Jeannin, 2001; Sudicky and McLaren, 1992); 3) double porosity model (Birk et al., 2006; Teutsch and Sauter, 1998); and 4) coupled continuum pipe flow or hybrid models (Liedl et al., 2003; Reimann et al., 2014).

In this study, to simulate groundwater flow and solute transport through the karst aquifer in the study area, a dual-continua model is used. Dual-continua models simulate flow through the matrix and conduit networks separately, but permit fluid exchange between the matrix and conduit networks. Both of the matrix and conduit networks contribute to groundwater flow in a dual permeability assumption for a karst aquifer (White, 1999; Worthington, 2015). Groundwater flow may take place in a non-Darcian (turbulent flow) regime within the conduit network.

Traditional numerical groundwater flow codes such as MODFLOW and FEFLOW typically do not consider dual porosity/permeability and non-Darcian flow behavior. However, the CFP

package added to MODFLOW (i.e., MODFLOW-CFP) was successfully used for numerical modeling of non-Darcian groundwater flow in karst media as a coupled continuum conduit network flow (Davis et al., 2010; DiFrenna et al., 2008; Gallegos et al., 2013; Hill et al., 2010; Reimann and Hill, 2009). MODFLOW-CFP contains three modules for modeling groundwater flow in karst media (Shoemaker et al., 2008b). In particular, two continua, matrix and conduit networks, are considered in module 1 referred to as CFPM1. Groundwater flow in the matrix (solved by the general groundwater flow equation based on Darcy's law) is coupled to groundwater flow in a discrete network of cylindrical pipes (solved by the Darcy-Weisbach and the Hagen-Poiseuille equations for turbulent and laminar flow conditions within the pipe network, respectively) (Reimann and Hill, 2009). Recently, a modified version of MODFLOW-CFPM1 referred to as CFPv2 has been introduced by Reimann et al. (2013) as a research version. In addition to a few enhancements in the flow subroutines, the major development in CFPv2 in comparison to MODFLOW-CFPM1 is subroutines related to heat and solute transport. CFPv2 considers solute transport in the conduit network by solving the one-dimensional advection-dispersion equation along the conduits. Moreover, a radial diffusion equation with retardation (due to linear sorption) is defined to evaluate the mass transfer between the conduits and the matrix (Reimann et al. 2013).

CFPv2 has been used for groundwater flow and mass transport modeling in karst conduit aquifer in different case studies (Karay and Hajnal, 2015; Reimann et al., 2014; Xu et al., 2015b, 2015a). In particular, Xu et al. (2015a) used CFPv2 to model the temporal variation of nitrate as a solute in a well-developed karst aquifer located in the Woodville karst plain, Florida. CFPv2 was also used by Karay and Hajnal (2015) for simulating the results of a laboratory bench-scale

model and concluded that the numerical model is capable in simulating both laminar and turbulent flow in karst aquifers. Xu et al. (2015b) developed a hybrid discrete-continuum groundwater model and mass transport model based on CFPv2. They applied the model for evaluating the interaction between seawater and freshwater in a karst aquifer consisting of conduit networks within the catchment area of two springs.

In this study, CFPv2 is utilized to support approaches for karst aquifer conceptualisation and to assess the geometrical characteristics of conduits in a karst aquifer located in the Zagros region, Iran. Linking of CFPv2 and OSTRICH (Optimization Software Toolkit for Research Involving Computational Heuristics), an optimization code, has not been previously attempted to investigate groundwater flow and solute transport for karst media even at the laboratory scale.

OSTRICH was developed by Matott (2013) as a model-independent, multi-algorithm optimization and calibration tool. A number of popular optimization algorithms such as the Genetic Algorithm (GA), Generalized Likelihood Uncertainty Estimation (GLUE) and Dynamically Dimensioned Search (DDS) algorithm have been embedded in OSTRICH. The DDS algorithm was developed for finding the global solution and frequently used for water resources optimization problems (Asadzadeh Esfahani, 2012; Tolson et al., 2014; Tolson and Shoemaker, 2008; Yen et al., 2016). The framework of DDS algorithm is based on the automatic calibration of higher dimensional problems, in particular, for watershed inverse problems (Yen et al., 2016). One benefit of DDS, which is the variable sampling of optimal parameter sets, results in better performance compared to other optimization algorithms in solving higher dimensional problems and to find the global solution (Tolson and Shoemaker, 2007; Yen et al., 2016, 2014).

In addition to acceptable convergence speed, DDS is designed to have less chance of being trapped within a local solution (Yen et al., 2014).

This study is considered as the first attempt to simultaneously apply CFPv2 and OSTRICH at the regional scale. Due to the scarcity of hydrodynamic information within the study area, four probable scenarios are assumed for the modeling approach. The OSTRICH code is coupled with CFPv2 to select the most reliable scenario among the four and to improve the knowledge of hydraulic parameters of the conduit network based on spring discharge and dye transport datasets.

Currently, dam foundation studies are being conducted in preparation for the future construction of the Maroon2 Dam, on a limestone formation in the study area (Fig. 1). Despite the successful construction of many dams at different karst regions throughout the world (Milanovic, 2011) there are several engineering problems and challenges for dam construction and other engineering activities in karst regions (Fazeli, 2007; Hiller et al., 2011; Milanovic, 2011; Parise and Gunn, 2007; Romanov et al., 2003). One of the key tasks for karst hydrogeologists is to identify solution conduits and cavities, their hydraulic parameters as well as their role in groundwater flow and solute transport. This is important as leakage from reservoirs and abutments of dams, especially those that are constructed in karst areas is very important and has been reported from several dam sites around the world (Milanovic, 2004). Moreover, leakage from a few of these dam sites persisted even after considerable treatment (e.g., impervious clay or asphalt, shotcrete and geotextile, etc.) and/or placement of underground watertight structures (e.g., grout curtain, cut-off wall, cavern plugging, etc.)

(Milanovic, 2011). Large values of leakage from dam sites have been attributed to high degrees of karst development.

In order to improve our understanding of the karst aquifer in the study area, this study attempts to evaluate the possible scenarios of conduit development and their hydrodynamic behaviour. There are several features that indicate the probable development of karst in the study area including significant elevation differences in hydraulic heads, only one major spring with a high amount of discharge at the discharge point, and existence of several sinkholes. The objectives of this study are: (1) to determine the degree of connection between the injection point and downstream spring via conduits; and (2) to better define the hydrodynamic characteristics of the conduit.

2. Geological setting

The study area is located in the Zagros Zone of the southern portion of Iran. The Zagros Zone is one of the five major structural zones in Iran (Alavi, 2004; Stöcklin, 1971). More than 90% of higher elevation land at the Zagros Zone are formed of karst limestone (Raeisi, 2002) and is divided into three sub-zones which are as follows: 1) Khuzestan Plain; 2) Thrust belt; and 3) Fold belt of the Zagros. The area of investigation is located in a fold belt sub-zone of the Zagros (Darvishzadeh, 1991). Anticlines and synclines in the study area have a north-west to south-east trend and is parallel with the general trend of the Zagros Zone.

A geological map of the study area is presented in Fig. 1. The exposed formations in the region, from oldest to youngest are: the Sarvak Formation (Cenomanian-Turonian) which is

comprised mainly of white limestone, the Gurp

includes marl, gray blue shale with interbeds of limestone layers, the Pabdeh Formation (Oligocene-Paleocene) composed of marl and gray shale with layers of clayish marine limestone, the Asmari Formation (Miocene) comprised of resistant brownish bisque limestone, and the alluvial deposits of the present age (Aghanabati, 2004). Among these formations, the Sarvak, Gurpi and Papdeh are abbreviated as Sv, Gu and Pd in Fig. 2 and are of more importance in the study area from a hydrogeological point of view. Based on remote sensing and field observations, it was found that no major faults are present in the study area. From a tectonic point of view, the folding structure in the formations of the region, have only led to the creation of some series of compressional joints at the crest of synclines and anticlines.

3. Hydrogeological setting

From a hydrogeological point of view, the major aquifer in the study area consists of the limestone of the Sarvak Formation. The Sarvak Limestone Aquifer (SLA) extends in the northwest-southeast direction of the Nil Anticline (Fig. 1). SLA is bounded by the marly formations of Pabdeh and Gurpi (Fig. 1). However, drilled boreholes in the vicinity of the Maroon River (Fig. 2) suggest that the limestone interlayer within the Gupri Formation has the potential to act as a local perched aquifer. The most important water resources in the region are the two permanent springs named Sarkur and Abriz (Fig. 2).

Sarkur Spring, with an annual average discharge of 5.2 m^3/s, is a major discharging point of SLA within the Nil Anticline, while Abriz Spring, with an average discharge of 0.05 m^3/s,

emerges as an overflow spring close to Sarkur Spring (Figs. 1 and 2). The general groundwater flow direction is thought to be towards Sarkur Spring as it is the main discharging point of the aquifer. However, there are no observation wells in SLA to draw an equipotential map to confirm this observation.

Seven shallow boreholes have been drilled within the Gurpi Formation close to the designed dam axis for geotechnical investigations (Fig. 2). The boreholes were not drilled deep enough to cross the SLA. However, groundwater levels in these boreholes reveal a local perched aquifer in the Gurpi Formation. It appears that the river water is recharging the local groundwater in the Gurpi Formation aquifer because the water level in the boreholes are measured to be 22 meters beneath the river level (Table 1).

In order to characterize the permeability of the dam foundation, water pressure tests (i.e., Lugeon test) have been conducted in seven shallow boreholes (Fig. 2). In particular, 134 Lugeon tests were conducted along consecutive 5-m long test sections throughout the entire depth of the boreholes (Table 1). Lugeon values in the boreholes range from 5 to 120 (equal to 5×10^{-7} to $1.2 \times 10^{-5}\ {}^{m}/_{s}$) with a geometric mean of 43.9 (equal to $4.4 \times 10^{-6}\ {}^{m}/_{s}$). It appears that large Lugeon values are related to the interbedded limestone layers of the Gurpi Formation.

Table 1: Hydrogeological characteristics of the shallow boreholes (Karimi, 2015).

Borehole	Depth (m)	Groundwater Level (m)	Difference between the groundwater and river levels (m)	Maximum Lugeon value	Minimum Lugeon value	Geometric mean of Lugeon value	No. of Lugeon tests
BH2	120	1185.9	-1.1	120	5	49.1	24
BH2-1	115	1163.6	-36.5	115	5	52.2	23
BH2-2	100	1141.0	-59.0	100	5	46.4	20
BH2-3	100	1229.5	-0.5	100	5	46.4	20
BH4	95	1183.1	-3.9	95	5	44.5	19
BH5	80	1158.6	-31.4	80	5	38.6	16
BH6	60	1169.9	-20.1	60	5	30.7	12

3.1. Water Balance

The general groundwater balance in the SLA is computed based on the water balance equation as:

$$\Delta S = \sum I - \sum O \quad (1)$$

where ΔS is change in storage of groundwater, and $\sum I$ and $\sum O$ are the sum of recharge (i.e., inflow) and discharge (i.e., outflow) components to the aquifer, respectively. All three terms in equation 1 are computed over a hydrogeological year from October 2014 to September 2015.

$\sum I$ is comprised of different inflow components such as subsurface inflow from the adjacent aquifer and recharge from precipitation and/or surface-water. $\sum O$ includes several outflow components such as subsurface outflow to an adjacent aquifer, the discharge through pumping wells and/or springs, and evapotranspiration from the water table (Raeisi, 2008).

Generally, karst aquifers are mainly recharged through rainfall. Due to the lack of detailed measurements of runoff and evapotranspiration in karst aquifers, the following equation is utilized to estimate the annual recharge to the karst aquifer:

$$I_P = A \times P \times C_{PF} \quad (2)$$

where I_P is volume of the annual recharge water from precipitation (m^3), A is the area of the aquifer (m^2), P is annual precipitation (m) and C_{PF} is the coefficient of precipitation fraction (dimensionless).

The area of the aquifer is determined based on: (1) the area of SLA (Fig. 2 and 3) which is bounded by the Pabdeh and Gurpi Formations as the impermeable boundary of the aquifer, (2) location of the emerging spring of SLA, and (3) considering all areas of the Sarvak Formation which have a higher elevation than the elevation of the spring outlet. Considering these factors, we estimate the area of SLA to be 239.5 km^2.

Due to the lack of rain-gauge stations over the area of SLA, a station (i.e., dam site station in Table 2) at an elevation of 1,297 meters above sea level (masl) was installed for measuring the monthly precipitation during the study period. However, topographic elevation ranges from 1,000 to more than 3,000 masl in the study area which causes temporal and spatial rainfall variability. In order to estimate the precipitation over the entire area of the SLA, a local,

empirical relationship between precipitation and elevation was used. The empirical relationship between precipitation-elevation in the study area was computed based on seven adjacent rain-gauge stations with their elevations ranging from 668 to 2,133 masl (Table 2). Since the duration of precipitation measurements is different in adjacent stations, a minimum coinciding period of 20 years was selected to extract the relationship between the mean annual precipitation and the elevation of adjacent stations (Fig. 3):

$$P = 0.22 \times Ele. + 281.65 \quad (3)$$

where P is annual precipitation (mm) and $Ele.$ is elevation (masl). The annual precipitation at the dam site station was 595 mm during the 2014 - 2015 water year (October 2014 to September 2015) which plots close to equation 3 (Fig. 4). It seems that equation 3 is suitable for estimating the mean annual precipitation over the area of SLA. Accordingly, the area weighted mean annual precipitation over the SLA is computed to be 560 mm by applying equation 3 to the topographic map covering the aquifer.

Table 2: Coordinates, mean annual rainfall and the available data period of selected rain-gauge stations in the vicinity of the study area.

Station	X (UTM)	Y (UTM)	Z (masl)	Mean annual rainfall (mm)	Data period (year)
Study area	479987	3430131	1297	595	1
Yasouj	552679	3394637	1816	827	34
Gachsaran	482377	3355736	726	445	32
Dehdasht	460132	3405664	793	491	21
Sisakht	448996	3411253	2133	697	21
Likak	414034	3424408	760	391	20
Emamzade-Jafar	498397	3352028	668	444	28
Mal-Khalife	524369	3462042	1749	610	21

C_{PF} is the fraction of precipitation which infiltrates to groundwater and is conceptually assumed as a fraction of spring discharge volume to the volume of total precipitation over unit time. Furthermore, a part of precipitation is converted to runoff or evapotranspiration. Since the monthly mean temperature ranges from 1 to 29°C with an annual mean of 19°C (Karimi, 2015), the runoff contribution is probably higher than evapotranspiration. Due to the lack of measurement or estimation of runoff and evapotranspiration over the SLA, C_{PF} was estimated based on exposed karst features and previous studies in the Zagros region (Karimi, 2015; Pezeshkpoor, 1991; Raeisi and Karami, 1997; Rahnemaie, 1994). Major surface karst features such as sinkholes, caves and grikes were mapped by Karimi (2015) according to field observations and remote sensing. A mean value of 0.57 with a range of 0.35 to 0.76 at the Gradole karst spring, Croatia (Bonacci, 2001), 0.67 with a range of 0.48 to 0.79 at Southern Apennines, Italy (Allocca et al., 2014), 0.57 with a range of 0.49 to 0.67 at the Dinaric karst, Croatia (Bonacci et al., 2006), 0.41 with a range of 0.27 to 0.94 at Sierra De Gador, Southern Spain (Li et al., 2011), and up to 0.9 at the Zagros Region, Iran (Raeisi, 2008) were reported for C_{PF} in different karst regions. Higher values of C_{PF} were assigned to highly developed karst areas characterized by a large number of sinkholes and heavy vegetation cover. An average value of 0.55 is assumed for the C_{PF} in the SLA based on visible surface karst features and reported values in similar karstic terrains. Taking into account the estimated values of A (239.5 km^2), P (560 mm) and C_{PF} (0.55) for the SLA, I_P is estimated to be approximately $110 \times 10^6 m^3$ (Karimi, 2015).

On the other hand, the SLA is only discharged by two permanent springs and there is no pumping well. Therefore, $\sum O$ in equation 1 can be replaced by spring discharge (O_S). Discharge of the main springs (e.g., Sarkur and Abriz) was sparsely gauged ten times by a current meter during the 2014 - 2015 water year. The spring discharge ranged from a minimum of 3 m^3/s in October, 2014 to a maximum of 7.5 m^3/s in February, 2015. A spring discharge of 5.1 m^3/s was measured three times in April, 2015 including: 1) prior to dye injection; 2) 10 days after injection; and 3) after finishing the dye sampling at the springs. Based on the time-weighted average of sporadically measured spring discharge, O_S from the SLA was computed to be 163 × 10^6 m^3.

It seems that the SLA is in a natural steady condition because there are not any impacts from pumping wells and the annual precipitation over the water balance period is close to the long-term mean annual precipitation based on seven adjacent rain-gauge stations. Assuming steady-state conditions, the change in groundwater storage can be assumed to be negligible over the hydrogeological year (Goldscheider and Drew, 2007). Assuming $\Delta \boldsymbol{S}$ =0, the volume of annual recharge from precipitation ($\boldsymbol{I_P}$) could be balanced by annual discharge water from the springs ($\boldsymbol{O_S}$). The difference of $\boldsymbol{O_S}$ and $\boldsymbol{I_P}$ in SLA is about 53 × 10^6 m^3 (equal to 1.7 m^3/s) over the hydrogeological year. Obviously, this difference demonstrates that the annual volume of discharging water from SLA exceeds the annual recharge by precipitation. Therefore, the spring is fed by additional water sources in addition to the annual recharge by precipitation.

In order to assess the Maroon River as a potential source of water that feeds the Sarkur Spring, river discharge was measured at five measurement stations along the river (abbreviated

from R1 to R5 in Fig. 2) which are located from upstream of the river to the designed dam site. Station R1 is furthest, while station R5 is in the close vicinity of the designed dam site. The distance between stations R1 and R5 is approximately 8 km along the river. The river discharge was measured six times at these stations with a current meter during the study period. These measurements revealed that river discharge generally diminishes from the upstream to downstream (Fig. 4). In particular, river discharge decreases between stations R1 and R5 from an average value of 8.0 to 5.8 m^3/s. Fig. 4 reveals that discharge ranges between 10.8 to 10.1 m^3/s on 16.02.2013 and between 4.0 to 1.9 m^3/s on 23.01.2014. As a result, river discharge decreases on average by 1.8 m^3/s from the upstream to downstream even during the dry season.

The measured discharge values at each station show extreme variations over time. It seems that the river discharge is mainly controlled by rainfall events. Normally, the rainy season starts from November and ends in late March or May in the study area. The measured discharge during the rainy season (dashed lines in Fig. 4) reveal a wide range of variations at all stations. However, river discharge reveals relatively smaller fluctuations at all stations during the dry season (solid lines in Fig. 4). On average, the variation of river discharge ranges from 1.5 to 2.4 m^3/s with an average of 1.9 m^3/s and from 6.7 to 8.5 m^3/s with an average of 7.9 m^3/s during the dry and the rainy seasons, respectively.

This suggests that recharge is taking place from the river to the underlying aquifer, which may be confirmed by: (1) the existence of several depressions thought to be sinkholes along the riverbank; and (2) the lower hydraulic head measured in shallow boreholes than the river level. Although recharge may be taking place locally based on data from the boreholes, we do not

know in detail how and where recharge is taking place along the rest of the river. However, it is reasonable to consider a recharge component from the river ($\boldsymbol{I_R}$) to the SLA. The annual amount of water loss from the river is estimated to be 56.7 × 10^6 m^3 that could probably serve as a resource for additional water supply that originates from Sarkur Springs.

Finally, coming back to equation 1, one could conclude that $\boldsymbol{O_S}$ (163 × 10^3 m^3) is approximately balanced by sum of $\boldsymbol{I_P}$ ($\boldsymbol{110 \times 10^6 m^3}$) and $\boldsymbol{I_R}$ (56.7 × 10^6 m^3).

3.2. Dye tracer test

After preliminary hydrogeological studies, 25 kilograms of Uranin dye was injected into a major depression close to the river, where it is labeled as the injection point in Fig. 2. This depression, considered to be a sinkhole, with a diameter of 2.5 m and a depth of 3 m, is located on the right side of the river at a distance of about 10 m from the riverbank. The sinkhole has developed in the alluvial sediments with thickness of less than 8 m overlying the Gurpi Formation. A mixture of 25 kg of dye with 600 L of water was instantaneously injected. In order to cause the dye to transport through the groundwater system, water was injected at a rate of 3 L/s into the sinkhole after dye injection for a duration of 8 hours.

In order to obtain dye concentrations at the sampling points, two types of sampling were conducted: 1) taking manual water samples and 2) setting packets of activated charcoal. Two springs including the Sarkur and Abriz, seven sections of the river (R2 to R8) and seven observation wells were selected for sampling and analysis of dye concentrations over a period of two months (Fig. 2). Water samples were taken at two-hour intervals during the first two

days after dye injection. The interval of water sampling was increased to 4, 8, 12, and 24 hours during four, six, eight and ten days after dye injection, respectively. Water samples were obtained daily over the remainder of the sampling period. Packets of activated charcoal were left beneath the flowing water at the outlet of the springs as well as different sections of the river and collected at weekly intervals. The activated charcoal is able to continuously sorb the dye tracer even at low dye concentrations during the sampling period (Field, 2005). Dye concentrations in the water and charcoal samples were measured with a spectrofluorometer (Shimadzu: Model: RF 5000-PC) with an accuracy of 0.001 ppb.

The results of the measured dye concentration at the sampling points were analyzed using the QTRACER2 program (Field, 2002) which is a program to quantitatively analyze dye tracer tests. The program has been designed for the easy computation of several parameters related to the conduit geometry and fluid dynamics such as total tracer recovery, mean residence time, mean tracer velocity, etc. (Field, 2002).

Based on the dye tracer test, it was found that the dye was not detected in any of the water samples, activated charcoal samples of the observation wells and sections of the river upstream of the dam axis. However, the dye was only observed at Sarkur spring with a maximum concentration of 7 ppb approximately three days after dye injection. Immediately after Sarkur Spring, the dye was detected at three stations along the river located downstream of Sarkur Spring due to mixing of the spring water with the river water.

Total tracer recovery (M_0), mean residence time ($\bar{t}$), and mean tracer velocity ($\overline{v}$) were computed based on the breakthrough curve of the dye tracer concentration at Sarkur Spring.

M_0 was computed to be 6.153 kg (i.e., equal to 24.6% of the injected mass) based on the following equation (Field, 2002):

$$M_0 = \int_0^{t_t} C_t \times Q_t \, dt \quad (4)$$

where C_t is concentration of dye in time t after dye injection and Q_t is the Sarkur spring discharge at time t. M_0 was computed over the time period of breakthrough curve that starts from 0 to t_t as the time over which the dye concentration reaches background levels. The $\bar{t}$ was estimated to be 111 hours based on equation 5 (Field, 2002):

$$\bar{t} = \frac{\int_0^{t_t} t \times C_t \times Q_t \, dt}{\int_0^{t_t} C_t \times Q_t \, dt} \quad (5)$$

while $\bar{v}$ was computed to be 96.11 m/h through Equation 6 (Field, 2002).

$$\bar{v} = \frac{\int_0^{t_t} \frac{l \times S_d}{t} \times C_t \times Q_t \, dt}{\int_0^{t_t} C_t \times Q_t \, dt} \quad (6)$$

where l is the straight-line distance between the injection point and the Sarkur spring (equal to 9,300 m) and S_d is the sinuosity factor. The conventional range of S_d in solution conduits is 1.3 to 1.5 (Field, 2002) and S_d is considered to be 1.35 in this study. Considering these results, one could conclude that there is clearly a hydraulic connection between the injection point and Sarkur spring.

3.3. Development of karst in the SLA

The development of karst is a complicated process controlled by geological, hydrological and hydrochemical processes. Favorable conditions for karst development in a hydrogeological setting takes place as a result of a combination of chemical (e.g., precipitation) and physical (e.g., relief) factors. Several hydrogeological factors such as the thickness of limestone layers, presence of fractures and rapid movement of groundwater may initiate the process of karst development (Ford and Williams, 2013).

The hydrogeological setting of the study area is suitable for karst development because several favorable factors have been identified. Firstly, there is considerable relief (i.e., approximately an elevation difference of 2,000 m between the recharge area of SLA in the peaks of the Nil anticline and Sarkur spring as the discharging point), which is able to act as a large driving force for rapid groundwater flow. Although $\overline{v}$ is estimated to be 96.11 mh^{-1} based on the dye tracer test, the maximum groundwater velocity may be higher. According to ASTM Standards (ASTM, 1998) the computed $\overline{v}$ is much higher than the ASTM criteria for classification of fast and slow groundwater flow. Therefore, it is concluded that groundwater in SLA may flow as fast conduit flow. Secondly, the average annual precipitation of 560 mm as the chemical driving force could initiate and enhance karst development in the SLA. Development of surface karst features in the study area especially several depressions and collapse features such as sinkholes could be considered as indications for karst development. Moreover, relatively high groundwater velocity and reported cavities and high Lugeon values at some sections of the boreholes are indirect subsurface evidences for karst development. Since the primary permeability of the matrix in limestone is relatively low, the high values of hydraulic conductivity obtained through borehole pressure tests may be attributed to secondary

permeability (i.e., fracture or conduit). The limitation of SLA by the presence of an impermeable layer that acts as no flow boundary, causes only one concentrated discharge point with an average discharge of 5.2 $m^3 s^{-1}$. Based on these observations, it could be concluded that the effects of sufficient annual precipitation and elevated relief superimpose within a thick bounded limestone to enhance the development of karst and create fast groundwater flow toward a discharge point.

4. Modeling approach

4.1. Numerical modeling with the CFPv2 model coupled with OSTRICH, a parameter estimation code

Recently, CFPv2 has been developed by Reimann et al. (2013), to simulate groundwater flow and solute transport in both conduits and the matrix. In addition to several updated flow subroutines in CFPv2 in comparison to MODFLOW-CFP, the major enhancement in CFPv2 includes several new solute transport subroutines (Reimann et al., 2013b). The physical and mathematical basis of groundwater flow and solute transport in CFPv2 were described in detail by Reimann et al. (2013) and Shoemaker et al. (2008b). In addition, the basic groundwater flow equation, the Darcy-Weisbach equation (Equ. 7) and the Hagen-Poiseuille equation (Equ. 8) are used for the computation of volumetric flow rate (Q) in a fully saturated one-dimensional turbulent and laminar pipe flow, respectively (Mcdonald and Harbaugh, 1988; Shoemaker et al., 2008b):

$$Q = A\sqrt{\frac{2\Delta h d g}{f \Delta l \, S_d}} \quad (7)$$

$$Q = A\frac{\rho g d^2 \Delta h}{32\mu \Delta l\, S_d} \quad (8)$$

where A is the cross-sectional area perpendicular to flow (L^2), Δh is head loss (L), Δl is distance (L), f is friction factor (dimensionless), d is pipe diameter (L), g is gravitational constant (LT^{-2}), S_d is sinuosity factor or tortuosity, ρ is water density (ML^{-3}), and μ is water dynamic viscosity ($ML^{-1}T^{-1}$).

In CFPv2, the one-dimensional advection-dispersion equation is used for evaluating solute transport in conduits as follows (Reimann et al., 2013b):

$$\frac{\partial c}{\partial t} = -v\frac{\partial c}{\partial x} + D_x\frac{\partial^2 c}{\partial^2 x} + S_c(x,t,c) \quad (9)$$

where *c* is the concentration (ML^{-3}), D_x is the dispersion coefficient (L^2T^{-1}), t is time (T), v is the mean groundwater velocity (LT^{-1}) and $S_c(x,t,c)$ is a source term (ML^{-3}) representing the increase of solute mass due to diffusive mass flux between the bulk water in the conduit and the matrix wall across the boundary layer (Reimann et al., 2013b).

CFPv2 considers advective-dispersive solute transport in the conduit as well as diffusive mass transfer between the conduit and the rock matrix (Reimann et al., 2013b). Conduits are defined as a network of pipes. Each segment of the pipe which is referred to as a tube consists of two end nodes. The flux exchange between the matrix and the conduit network nodes is computed as follows:

$$Q_{ex} = \alpha_{i,j,k}(h_n - h_{i.j,k}) \quad (10)$$

where Q_{ex} is the volumetric flow exchange rate (L^3T^{-1}), $\alpha_{i,j,k}$ is the pipe conductance at cell i,j,k (L^2T^{-1}) and h_n and $h_{i,j,k}$ are the heads at pipe node n and the head in the cell i,j,k, respectively.

According to equations 7 to 10, several variables (e.g., conduit diameter, friction factor, hydraulic conductivity, pipe conductance, dispersion coefficient, tortuosity and so on) are necessary for groundwater flow and solute transport modeling using CFPv2. However, most of these variables are unknown and have not been measured in the study area. Moreover, the number of measured parameters related to the hydraulic behaviour of the karst aquifer in the study area are inadequate and only include spring discharge, dye tracer breakthrough curve, river discharge and annual rainfall. In order to overcome the problem of having a large number of model parameters and a limited number of measured field observations, an optimization approach is used to calibrate the model based on available field data. The authors are aware that the selected optimization process is inherently ill-posed and the unique solution may not be obtained. However, we tried to reduce the ill-posed condition for this case study by defining four most probable hydrogeological scenarios and considering new data from the water balance study and the dye tracer breakthrough curve (McLaughlin and Townley, 1996).

OSTRICH is an optimization software that provides a Weighted Sum of Square Error (WSSE) objective function to minimize the difference between the measured field parameters and the model outputs as follows:

$$WSSE = \sum_{i=1}^{N} [w_i(Z_{sim,i} - Z_{obs,i})]^2 \quad (11)$$

where w_i is the weight assigned by the user to the *i*-th observation, *N* is the total number of observations, $Z_{sim,i}$ and $Z_{obs,i}$ are the *i*-th simulated and measured observation, respectively.

OSTRICH is coupled and executed with the CFPv2 model through several text-based input and output files. In order to simultaneously execute both models, the format of their input and output files should be consistent. Both of the models support the ASCII file format. However, the format of CFPv2's output files for concentration of the dye and spring discharge are automatically modified by an extra batch file to print only the simulated values coinciding with the measured times. These modified files are launched by OSTRICH for computing the objective function. The procedure for optimization is presented in a flowchart (Fig. 5).

This procedure is separately applied to the four assumed scenarios in the study area. The scenarios are introduced in the next section. The accuracy of each scenario to simulate the dye concentration or the spring discharge is evaluated through the Mean Relative Difference Error (MRDE) and Mean Square Error (MSE) criteria:

$$MRDE = \left(\frac{1}{N}\sum_{i=1}^{N}\left|\frac{Z_{obs,i} - Z_{sim,i}}{Z_{obs,i}}\right|\right) \times 100 \quad (12)$$

$$MSE = \frac{1}{N}\sum_{i=1}^{N}(Z_{obs,i} - Z_{sim,i})^2 \quad (13)$$

where $Z_{obs,i}$ and $Z_{sim,i}$ are the observed and simulated values of concentration or discharge of the Sarkur spring at time *t* and *N* is the number of measured concentration or discharge data.

4.2. Conceptual model and the scenarios

The schematic model of the movement of the dye between the injection point (the sinkhole) and Sarkur Springs is presented in Fig. 6. Since the dye was not observed in any of the sampled water as well as through the activated charcoal samples of the shallow boreholes and the river sections, it can be concluded that the dye must have moved downward through the limestone interlayers of the Gurpi Formation up-gradient of the boreholes. On the other hand, the river water appears to discharge into the Gurpi Formation due to the average of 21-meter difference between the river and the local groundwater levels as well as due to the observed decrease in river discharge from R1 to R5 by an average of 1.8 $\boldsymbol{m^3 s^{-1}}$ (Fig. 4). Based on these observations, it appears that the dye passes through the Gurpi Formation, mixes with groundwater flowing through the SLA and finally emerges from Sarkur Spring.

According to available indications, conduit flow path in the SLA is most probable, but the dye transport path from the injection point to the SLA is not exactly known. In order to assess the type and diameter of conduit flow path between the injection point and the spring, four scenarios are considered (Fig. 7): 1) lack of a major conduit (Case S0), and a major conduit developed at 2) 0 m; 3) 1,000 m; and 3) 2,000 m from the injection point to the downgradient spring (Cases S1, S2 and S3, respectively). Case S0 is assumed to be an equivalent porous medium and the only difference between Cases S1, S2 and S3 is the location and number of pipes and nodes of the major conduit.

In order to develop a regional groundwater flow and solute transport model for the various scenarios, the CFPv2 code (Reimann et al., 2013b) is selected. ModelMuse (Winston,

2009) as a graphical user interface (GUI) was used to prepare the input files to run CFPv2. The SLA is treated to be a regional unconfined aquifer that is homogenous and isotropic. The model area is discretized into 10 rows and 39 columns with each cell having dimensions of 1,000 × 1,000 m due to the lack of detailed spatial data (Fig. 8). Although in a few studies the grid cell size has been selected to be smaller such as 360 m (Ghasemizadeh et al., 2016) and 610 m (Dufresne and Drake, 1999), Faunt et al. (2004) and Welsh (2000) selected a grid size of 1,500 m and 5,000 m for their regional groundwater model, respectively. The range of grid sizes for typical regional groundwater flow models reviewed could vary from 6 to 25 km (Zhou and Li, 2011).

In terms of boundary conditions, a constant value of 1,000 m is assigned to the bottom elevation of the model area. A gentle topographic gradient of 0.005 is assumed for the top elevation of the grid cells with the elevation of Sarkur spring set as the lowest topographic elevation. The maximum thickness of the SLA is controlled to be less than 350 m in the model domain. A no-flow boundary is assumed for the side boundaries of the model domain because the SLA is bounded by impermeable layers.

The general groundwater flow direction is toward the spring throughout the entire model domain. A hydraulic gradient of 0.001 is assumed for the generation of hydraulic head in the model cells as an initial condition. Values of net precipitation and distributed infiltration from the river are assigned as sources of recharge to the model domain. Two different recharge rates are assigned to the model domain: (1) a value of $\mathbf{1 \times 10^{-8}\ m\ day^{-1}}$ to the entire model area as net precipitation; and (2) a value of $\mathbf{1 \times 10^{-7} m\ day^{-1}}$ to the cells that cover the areas of the river that contribute to recharge (Fig. 8). Only one discharge point, Sarkur spring, is

assumed for the model and treated as a drain in CFPv2. An initial constant value of 0.01 $\boldsymbol{m^1}$ $\boldsymbol{day^{-1}}$ is assumed for the horizontal hydraulic conductivity. Since the duration of the breakthrough curve in Sarkur spring is about 10 days, the numerical model was executed for steady state condition that have two stress periods and 240 time steps with a length of one hour for each time step. Spring discharge was treated to be a constant with a value 5.2 $\boldsymbol{m^3 s^{-1}}$ during the dye tracer test. A conduit which is discretized into 15 pipes and 16 nodes was initially assumed to simulate the hydraulic connection between the injection point of the dye and the spring.

5. Results and discussion

Firstly, the CFPv2 model was implemented for the homogeneous and isotropic scenarios, and only the spring discharge and volumetric budget of the SLA were considered for controlling of the model outputs and manual calibration. Then, with the simultaneous implementation of both CFPv2 and OSTRICH, we tried to improve the knowledge of key parameters that control groundwater flow and solute transport (Fig. 5). The initial parameters used for optimization and their range of variation are given in Table 3. In order to improve the optimization process and to prevent the convergence of solution to a local minimum, the initial values of the parameters were randomly changed by OSTRICH. The optimization model converged through consideration of at least 110 iterations for the DDS algorithm as implemented in OSTRICH for each scenario.

Table 3: Initial values of the optimized parameters in CFPv2 and their range of variation.

Parameter	Unit	Lower limit	upper limit	Initial value
Conduit diameter	m	1.00E-01	5.00E+00	1.50E+00
Tortuosity	unit-less	1.00E+00	1.90E+00	1.20E+00
Pipe conductance (Exchange coefficient)	m^2s^{-1}	1.00E-05	1.00E-01	1.00E-03
Conduit roughness	m	1.00E-04	1.00E+00	1.00E-03
Diffusion coefficient	m^2s^{-1}	1.00E-10	1.00E-07	1.00E-08
Recharge from the river	ms^{-1}	1.00E-09	1.00E-05	1.00E-07
Hydraulic conductivity	ms^{-1}	1.00E-05	1.00E+02	1.50E+00

5.1. Reliability of the scenarios

The reliable scenario and realistic optimal values of the specified parameters are selected through the assessments of: (1) values of the objective function, (2) values of MRDE and MSE, and (3) comparisons of the measured and simulated breakthrough curve, spring discharge, mean groundwater velocity and percent of dye recovery.

The objective function is defined to minimize the differences between the measured values of the spring discharge and dye concentration in the spring. Although the objective functions of S1, S2 and S3 are found to decrease smoothly to an acceptable value of less than 0.01 at the end of the iteration, in general, S1 yields the lowest value of 0.001 (Fig. 9). However, there is no decreasing trend in the difference between the observed and simulated data in S0 even at the end of iteration (Fig. 9). Therefore, we conclude that S1 provides the closest results to the measured data.

The value of MRDE and MSE related to the measured spring discharge and dye concentrations for each of the scenarios are presented in Fig. 10. The highest values of MRDE and MSE are found for S0 regarding the simulated dye concentration as well as spring

discharge. Despite the low value of MRDE based on the spring discharge in S3, this scenario revealed unreliable behavior in simulating the dye concentration (Fig. 10A).

The values of MRDE and MSE computed for S2 and S3 are in an acceptable range and their hydrodynamic characters are relatively similar to the actual flow condition, but S1 shows smaller MRDE and MSE values. Therefore, S1 is optimized to a better set of the parameters that allows for the more accurate simulation of groundwater flow and solute transport in the study area.

A comparison of the measured and simulated breakthrough curves for each scenario is provided in Fig. 11. The lack of ability in S0 and S3 to reproduce the breakthrough curve reveals that these scenarios are not feasible in simulating groundwater flow and solute transport in the study area (Fig. 11). Moreover, S2 is also not reliable because the simulated breakthrough curve is significantly different from the measured curve. In contrast to the other cases, S1 yields a breakthrough curve that is comparable to the measured one (Fig. 11).

Table 4 provides a comparison of the dye tracing test condition and the different scenarios in terms of spring discharge and the characteristics of breakthrough curve. Since S0 and S3 was not able to reproduce the breakthrough curve (Fig. 11), parameters related to the breakthrough curve (i.e., peak concentration, time to peak concentration, mean groundwater velocity and the dye recovery) are not provided for these scenarios in Table 4. It seems that not building in a conduit for S0 by treating the karst aquifer to be a single continuum results in the lack of dye tracer transport from the injection point to the spring. Likewise, the lack of connection of a defined conduit to the injection point in S3 yields results similar to S0.

Moreover, S2 yields good results for the prediction of spring discharge, but fails to predict the transport behavior of the dye tracer. On the other hand, S1 yields excellent results in terms of spring discharge, peak concentration and time to peak concentration (Table 4), while the mean groundwater velocity is slightly overestimated. Meanwhile, S2 yields a mean groundwater velocity that is two times higher than that inferred from the dye tracer test.

The mean groundwater velocity is computed based on time to peak concentration and the distance between the injection point and the spring. Therefore, the mean groundwater velocity is estimated based on the straight line distance between the injection point and the spring (equal to 10 km for the case study) and the sum of tube lengths in the mode domain (equal to 14 km for S1). This contributes to an overestimation of the mean groundwater velocity in S1 versus the field case. As a result, the computed mean groundwater velocity in S1 shows a difference of 30% in comparison to the field data. Moreover, the total dye recovery in S1 shows a small increase in comparison to the dye test condition (Table 4). This difference is due to the area under the breakthrough curve which is quantified by implementing Equation 4 over the simulated breakthrough curve in S1 (Fig. 11). Overall, the difference between S1 and the field data, in comparison to the other scenarios, is quite small that it can be considered to be a reliable scenario for simulating available data. The lack of ability for S0 and S3 in reproducing the breakthrough curve at the spring may be considered as an indication of the presence of a major conduit between the injection and spring discharge points.

Table 4: Comparison of measured and simulated spring discharge, time to peak concentration, mean groundwater velocity, and dye recovery for different scenarios.

Scenario	Spring discharge ($m^3 s^{-1}$)	Time to peak concentration (h)	Peak concentration (ppb)	Mean groundwater velocity ($m h^{-1}$)	Dye recovery (%)
S0	5.08	nd	nd	nd	nd
S1	5.2	111.1	6.31	126.1	26
S2	5.21	75.8	0.47	184.3	1.5
S3	5.19	nd	nd	nd	nd
Dye tracing test	5.2	110.8	6.45	96.1	24

nd: not determined

5.2. Assessment of the optimized parameter values

The optimized values of the specified parameters (i.e., conduit diameter, tortuosity, conduit roughness, exchange coefficient, diffusion coefficient, hydraulic conductivity, and recharge rate from the river) in each scenario are presented in Table 5. Except the recharge rate from the river, the rest of these parameters have not been controlled by the field data due to lack of measured data related to these parameters in the study area. However, the hydrogeological conditions of the study area and parameter values from the literature have been used to assess the reliability of parameters.

Cases S1, S2, and S3 yielded optimized conduit diameter values of 3.06, 2.91 and 4.74 m, respectively. Case S0 excluded the presence of conduits and the related parameters as the karst aquifer was treated to be a uniform, single continuum. The conduit diameter in S3 was estimated to be about 1.6 times larger than S1 and S2 resulting in S3 not being able to reproduce the breakthrough curve and spring discharge (Fig. 11). Considering the better performance of S1 in comparison to S2 in simulating field data (Figs. 10 and 11) and the 2.5 m diameter of the sinkhole at the dye injection point, a conduit diameter of approximately 3 m

appears to be reasonable in simulating groundwater flow and solute transport in the study area.

The optimized values of tortuosity is shown to be low in variability with an average value of 1.44. Tortuosity or sinuosity factor is defined as a unitless coefficient (typical values of 1.3 – 1.5 in karst aquifers) that is multiplied with the straight-line distance between the injection and sampling points to estimate a more probable transport distance for the dye tracer experiment. Although tortuosity could range from 1 to 3 (Field, 2002; Worthington, 1991), the optimized value of 1.44 is within the range of suggested values of 1.27 (Aydin et al., 2014), 1.3 to 1.5 (Field, 2002) and 1.7 (Assari and Mohammadi, 2017).

Generally, conduit roughness, exchange coefficient, and the diffusion coefficient are estimated through model calibration as determining these parameters in the field is not straightforward requiring accurate instrumentation and a large budget. Here, conduit roughness is optimized to be approximately the same for S1, S2, and S3 with an average of 3.91 $\times 10^{-2}$m. In addition, the optimized exchange coefficient is similar for S1 and S2 and is three times more than S3 (i.e., $0.78 \times 10^{-2}\, m^2 s^{-1}$). Moreover, the optimized value of diffusion coefficient varies by one order of magnitude for the scenarios considered (Table 5). The comparison of conduit roughness, exchange coefficient, and diffusion coefficient to those from the literature (Reimann et al., 2013a, 2011; Shoemaker et al., 2008b), suggests that S1 yields the most realistic parameters among all cases.

The hydraulic conductivity in karst aquifers often exhibits a very wide range. In this study, the optimized values range from 0.67 to 55.14 md^{-1} (Table 5). In particular, hydraulic conductivity in S1 is estimated to be 10 md^{-1}. Even though the value of 10 md^{-1} may seem

to be high for fracture-matrix continuum, the value may be acceptable considering the fact that the model assumes the presence of a single major conduit within the aquifer and the other secondary porosities like micro joints/fractures are treated to be part of a single continuum with the matrix in this modeling study.

The optimized value for the recharge rate from the river in S0 and S3 are largely different from the water balance in the study area (section 3-1). However, the optimized value in S1 and S2 are within the range of the water balance study (Table 5).

Table 5: Optimized values for the selected parameters.

Scenario	Conduit diameter (m)	Tortuosity (unit-less)	Conduit roughness ($\times 10^{-2}$m)	Exchange coefficient ($\times 10^{-2} m^2 s^{-1}$)	Diffusion coefficient ($\times 10^{-7} m^2 s^{-1}$)	Hydraulic conductivity (md^{-1})	Recharge rate from the river ($\times 10^{-6} md^{-1}$)
S0	nd	Nd	nd	nd	0.44	8.83	2.00
S1	3.06	1.53	3.78	2.45	9.71	10.15	1.13
S2	2.91	1.35	4.07	2.00	0.77	0.67	1.03
S3	4.74	1.45	3.88	0.78	6.72	55.14	0.77

nd: not determined

5.3. Limitations of the model and future improvements

Although it may seem at first glance that our model is ill-posed, it provides a better understanding of groundwater flow system in the study area. Of course, the amount of available data for this study is small compared to a few other groundwater modeling studies in karst terrain (e.g., Morales et al., 2017; Xu et al., 2015a). However, the basic hydrogeological framework and most crucial data such as spring discharge and breakthrough curve are available

for this site. Our study attempts to overcome data limitations by making assumptions and simplifications to the model.

The first limitation of modeling approach in the study area is the lack of spatial and temporal water table data. However, unique hydrogeological characteristics of the studied karst aquifer (i.e., no flow boundaries, only one discharge point, direct recharge by the river, no pumping wells, etc.) provide some degree of knowledge that allows one to choose appropriate assumptions and to simplify the conceptual model of groundwater flow and solute transport at this site (see section 4.2). In addition, the modeling approach was supported by enough data on spring discharge.

The second limitation is due to the scarcity of solute transport data. A more accurate solute transport model could have been constructed through the availability of additional monitoring points of dye concentrations between the injection point and the spring. Nevertheless, the optimization routine was utilized to find the optimal set of parameters allowing for the model outputs (i.e., the spring discharge and tracer breakthrough curve) to match the measured field data.

It should be stressed that S1 is considered to be the best scenario in this study, but we fully acknowledge that this is just one scenario among an infinite number of possibilities, thus caveats should be provided that more studies are needed to map the conduit system to further constrain the inverse problem. In fact, the behaviour of the groundwater flow system is mainly examined by spring discharge and a dye tracing test in the current study. A more accurate groundwater model will require additional information from new boreholes, more dye tracing

tests, measurements of hydraulic and dye tracer concentrations throughout the watershed, and extensive spatial and temporal measurements of components of water balance equation. Then perhaps the modeling results may be further improved and become more representative of site conditions. Nevertheless, our new approach (linking of CFPv2 and OSTRICH) provides new insight to the study area and proves the existence of a major conduit, most probably with a diameter of 3 m, although the exact location of the conduit remains unknown. Field geophysical (Chalikakis et al., 2011; McGrath et al., 2002; Šumanovac and Weisser, 2001) and hydraulic tomography (e.g., Illman et al., 2009; Zha et al., 2016, 2015; Wang et al., 2017; Fischer et al., 2018) surveys may be necessary to map the conduit geometry more accurately.

6. Findings and Conclusions

This study presented a coupling of CFPv2 and OSTRICH to simulate groundwater flow and solute transport in a karst region and to automatically estimate model parameters. The case study includes a karst aquifer (i.e., SLA) which recharges through net precipitation over the modeled region and infiltration of surface water from the Maroon River, while discharging at a single point (i.e., Sarkur spring). Despite the lack of detailed hydrochemical and isotopic data, the modeling tools utilized in this study allowed for the parameter estimation of conduit geometrical characteristics and the surrounding fracture-matrix continuum based on available hydrogeological and dye tracing data sets. The appearance of the dye at Sarkur Spring confirms the existence of a hydraulic connection between the injection point and the spring. At this study area, we conclude that there is a well-developed conduit within the karst aquifer based

on the following measured data: 1) high groundwater velocity of 96.11 m^1h^{-1}; 2) an average loss of river discharge (1.8 m^3s^{-1}) into the SLA as one moves down the river; 3) concentrated recharge through sinkholes; and 4) the existence of a single spring with an average discharge of 5.2 m^3s^{-1}. However, the hydraulic parameters of the conduit as well as its geometry are not clear.

Four scenarios were assumed to reconstruct the groundwater flow and solute transport conditions within the study area as well as the conduit. In addition to modeling of regional groundwater flow and solute transport using CFPv2, an optimization code, OSTRICH is used to help select the most reliable scenario. This study is the first attempt to link CFPv2 to OSTRICH, an optimization code to model groundwater flow and solute transport of a karst aquifer.

The selected scenarios provide important insights about the karst aquifer. In particular, our results suggest that scenario S1, which assumes the presence of a developed conduit with an average diameter of 2.9 m shows the most reliable reconstruction of the hydraulic condition of the study area. S1 simulates the spring discharge and the dye breakthrough curve with lower MRDE and MSE in comparison to the other scenarios. Moreover, the optimized values for the parameters in S1 are within an acceptable range reported in the literature.

Fortunately, results of this research (i.e., inferring the presence of a major conduit between the upstream and downstream areas of the designed dam site) and also new geotechnical studies (not included in this study) prevented the construction of the Maroon2 Dam in this area. Although this study does not cover karst engineering-related issues encountered at the site, the likelihood of a significant dam leakage potential through the

modeled conduit (i.e., through Case S1) can be envisioned based on our numerical modeling results. In particular, it is quite likely that the construction of the dam and impounding of water will significantly increase the hydraulic head gradient, leading to an increase in leakage potential that could potentially result in a catastrophic failure of the dam at this site.

In order to prevent such failures, there is a critical need to more accurately map karst features including conduits, their connectivity, network characteristics as well as hydraulic parameters that control groundwater flow and solute transport. Therefore, there is a need for new characterization approaches which could involve geophysical and hydraulic tomography surveys.

Finally, this study emphasizes the application of integrated hydrogeological, modeling and optimization approaches for the improved understanding of karst aquifers and hydraulic parameters of the conduits even when available data are limited.

Acknowledgment

The first author would like to acknowledge Shiraz University for financial support during field works and sabbatical leave at University of Waterloo. This research also was partly supported by Regional Water Authority of Kohgiloye and Boyerahmad Province, Iran. The second author acknowledges the support from Natural Sciences and Engineering Council of Canada through the Discovery grant which made this collaboration with the first author possible. We are also grateful for constructive and useful comments and suggestions from the editor and two anonymous reviewers.

References

Aghanabati, A., 2004. Geology of Iran. Geological survey of Iran.

Alavi, M., 2004. Regional stratigraphy of the Zagros fold-thrust belt of Iran and its proforeland evolution. Am. J. Sci. 304, 1–20. https://doi.org/10.2475/ajs.304.1.1

Allocca, V., Manna, F., De Vita, P., 2014. Estimating annual groundwater recharge coefficient for karst aquifers of the southern Apennines (Italy). Hydrol. Earth Syst. Sci. 18, 803–817. https://doi.org/10.5194/hess-18-803-2014

Annable, W.K., Sudicky, E.A., 1998. Simulation of karst genesis: hydrodynamic and geochemical rock-water interactions in partially-filled conduits. Bull Hydrogéol 16, 211–221.

Asadzadeh Esfahani, M., 2012. Developing parsimonious and efficient algorithms for water resources optimization problems - University of Waterloo. University of Waterloo.

Assari, A., Mohammadi, Z., 2017. Assessing flow paths in a karst aquifer based on multiple dye tracing tests using stochastic simulation and the MODFLOW-CFP code. Hydrogeol. J. 25, 1679–1702. https://doi.org/10.1007/s10040-017-1595-z

Aydin, H., Ekmekçi, M., Soylu, M.E., 2014. Effects of sinuosity factor on hydrodynamic parameters estimation in karst systems: a dye tracer experiment from the Beyyayla sinkhole (Eskişehir, Turkey). Environ. Earth Sci. 71, 3921–3933. https://doi.org/10.1007/s12665-013-2777-1

Bakalowicz, M., 2005. Karst groundwater: a challenge for new resources. Hydrogeol. J. 13, 148–

160. https://doi.org/10.1007/s10040-004-0402-9

Barrett, M., Charbeneau, R., 1996. A parsimonious model for simulation of flow and transport in a karst aquifer.

Bauer, S., Liedl, R., Sauter, M., 2003. Modeling of karst aquifer genesis: Influence of exchange flow. Water Resour. Res. 39. https://doi.org/10.1029/2003WR002218

Birk, S., Liedl, R., Sauter, M., 2006. Karst Spring Responses Examined by Process-Based Modeling. Ground Water 44, 832–836. https://doi.org/10.1111/j.1745-6584.2006.00175.x

Birk, S., Liedl, R., Sauter, M., Teutsch, G., 2003. Hydraulic boundary conditions as a controlling factor in karst genesis: A numerical modeling study on artesian conduit development in gypsum. Water Resour. Res. 39, SBH 2-1-SBH 2-14. https://doi.org/10.1029/2002WR001308

Bonacci, O., 2001. Monthly and annual effective infiltration coefficients in Dinaric karst: example of the Gradole karst spring catchment. Hydrol. Sci. J. 46, 287–299. https://doi.org/10.1080/02626660109492822

Bonacci, O., Jukić, D., Ljubenkov, I., 2006. Definition of catchment area in karst: Case of the rivers Krčić and Krka, Croatia. Hydrol. Sci. J. 51, 682–699. https://doi.org/10.1623/hysj.51.4.682

Borghi, A., Renard, P., Cornaton, F., 2016. Can one identify karst conduit networks geometry and properties from hydraulic and tracer test data? Adv. Water Resour. 90, 99–115. https://doi.org/10.1016/j.advwatres.2016.02.009

Cacas, M.C., Ledoux, E., de Marsily, G., Tillie, B., Barbreau, A., Durand, E., Feuga, B., Peaudecerf, P., 1990. Modeling fracture flow with a stochastic discrete fracture network: calibration and validation: 1. The flow model. Water Resour. Res. 26, 479–489. https://doi.org/10.1029/WR026i003p00479

Chalikakis, K., Plagnes, V., Guerin, R., Valois, R., Bosch, F.P., 2011. Contribution of geophysical methods to karst-system exploration: an overview. Hydrogeol. J. 19, 1169–1180. https://doi.org/10.1007/s10040-011-0746-x

Darvishzadeh, A., 1991. Geology of Iran. Amirkabir Publication (Persian).

Davis, H., Katz, B., Griffin, D., 2010. Nitrate-N Movement in Groundwater from the Land Application of Treated Municipal Wastewater and Other Sources in the Wakulla Springs Springshed, Leon and Wakulla Counties, Florida, 1966–2018.

DiFrenna, V.J., Price, R.M., Savabi, M.R., 2008. Identification of a hydrodynamic threshold in karst rocks from the Biscayne Aquifer, south Florida, USA. Hydrogeol. J. 16, 31–42. https://doi.org/10.1007/s10040-007-0219-4

Dufresne, D.P., Drake, C.W., 1999. Regional groundwater flow model construction and wellfield site selection in a karst area, Lake City, Florida. Eng. Geol. 52, 129–139. https://doi.org/10.1016/S0013-7952(98)00066-0

Faunt, C.C., Sweekind, D.S., Belcher, W.R., 2004. Three-dimensional Hydrogeological Framework Model, Chapter E of Death Valley Regional Groundwater Flow System, Nevada and California-Hydrogeological Framework and Transient Groundwater Flow Model.

https://doi.org/5205

Fazeli, M.A., 2007. Construction of grout curtain in karstic environment case study: Salman Farsi Dam. Environ. Geol. 51, 791–796. https://doi.org/10.1007/s00254-006-0397-8

Field, M.S., 2002. QTRACER2 program for tracer-breakthrough curve analysis for karst aquifers and other hydrologic systems. National Center for Environmental Assessment--Washington Office, Office of Research and Development, U.S. Environmental Protection Agency.

Fischer, P., Jardani, A., Lecoq, N., 2018. Hydraulic tomography of discrete networks of conduits and fractures in a karstic aquifer by using a deterministic inversion algorithm. Adv. Water Resour. 112, 83–94. https://doi.org/10.1016/j.advwatres.2017.11.029

Ford, D.C., Williams, P., 2013. Karst hydrogeology and geomorphology. Wiley.

Gallegos, J.J., Hu, B.X., Davis, H., 2013. Simulating flow in karst aquifers at laboratory and sub-regional scales using MODFLOW-CFP. Hydrogeol. J. 21, 1749–1760. https://doi.org/10.1007/s10040-013-1046-4

Ghasemizadeh, R., Yu, X., Butscher, C., Padilla, I.Y., Alshawabkeh, A., 2016. Improved regional groundwater flow modeling using drainage features: a case study of the central northern karst aquifer system of Puerto Rico (USA). Hydrogeol. J. 24, 1463–1478. https://doi.org/10.1007/s10040-016-1419-6

Goldscheider, N., Drew, D., 2007. Methods in Karst Hydrogeology: IAH: International Contributions to Hydrogeology, 26.

Graf, T., Therrien, R., 2007. Variable-density groundwater flow and solute transport in irregular

2D fracture networks. Adv. Water Resour. 30, 455–468. https://doi.org/10.1016/j.advwatres.2006.05.003

Hill, M.E., Stewart, M.T., Martin, A., 2010. Evaluation of the MODFLOW-2005 conduit flow process. Ground Water 48, 549–559. https://doi.org/10.1111/j.1745-6584.2009.00673.x

Hiller, T., Kaufmann, G., Romanov, D., 2011. Karstification beneath dam-sites: From conceptual models to realistic scenarios. J. Hydrol. 398, 202–211. https://doi.org/10.1016/j.jhydrol.2010.12.014

Illman, W.A., Liu, X., Takeuchi, S., Yeh, T.-C.J., Ando, K., Saegusa, H., 2009. Hydraulic tomography in fractured granite: Mizunami Underground Research site, Japan. Water Resour. Res. 45. https://doi.org/10.1029/2007WR006715

Jeannin, P.-Y., 2001. Modeling flow in phreatic and epiphreatic Karst conduits in the Hölloch Cave (Muotatal, Switzerland). Water Resour. Res. 37, 191–200. https://doi.org/10.1029/2000WR900257

Karay, G., Hajnal, G., 2015. Modelling of Groundwater Flow in Fractured Rocks. Procedia Environ. Sci. 25, 142–149. https://doi.org/10.1016/j.proenv.2015.04.020

Karimi, M., 2015. Hydrogeology and Dye tracing of Maroon2 Dam site. Shiraz University, Iran.

Kass, W., Behrens, H., 1998. Tracing technique in geohydrology. Belkema.

Kaufmann, G., Braun, J., 2000. Karst Aquifer evolution in fractured, porous rocks. Water Resour. Res. 36, 1381–1391. https://doi.org/10.1029/1999WR900356

Keeler, R., Zhang, Y., 1997. Modeling of groundwater flow in a fractured-karst aquifer in the Big

Springs Basin, Iowa. Geol. Soc. Am., Abs. Programs 29, 1–25.

Kiraly, L., 1998. source qui doit être utilisée pour toute référence à ce travail 77–98.

Lapcevic, P.A., Novakowski, K.S., Sudicky, E.A., 1999. The interpretation of a tracer experiment conducted in a single fracture under conditions of natural groundwater flow. Water Resour. Res. 35, 2301–2312. https://doi.org/10.1029/1999WR900143

Larocque, M., Banton, O., Ackerer, P., Razack, M., 1999. Determining Karst Transmissivities with Inverse Modeling and an Equivalent Porous Media. Ground Water 37, 897–903. https://doi.org/10.1111/j.1745-6584.1999.tb01189.x

Li, X.Y., Contreras, S., Solé-Benet, A., Cantón, Y., Domingo, F., Lázaro, R., Lin, H., Van Wesemael, B., Puigdefábregas, J., 2011. Controls of infiltration-runoff processes in Mediterranean karst rangelands in SE Spain. Catena 86, 98–109. https://doi.org/10.1016/j.catena.2011.03.003

Liedl, R., Sauter, M., Hückinghaus, D., Clemens, T., Teutsch, G., 2003. Simulation of the development of karst aquifers using a coupled continuum pipe flow model. Water Resour. Res. 39. https://doi.org/10.1029/2001WR001206

Matott, L., 2013. an Optimization Software Tool, Documentation and User's Guide, Version 17.12.19. Univ. Buffalo Cent. Comput. Res.

Mcdonald, M.G., Harbaugh, A.W., 1988. A MODULAR THREE-DIMENSIONAL Fl N ITE-DI FFERENCE GROUND-WATER FLOW MODEL.

McGrath, R.J., Styles, P., Thomas, E., Neale, S., 2002. Integrated high-resolution geophysical

investigations as potential tools for water resource investigations in karst terrain. Environ. Geol. 42, 552–557. https://doi.org/10.1007/s00254-001-0519-2

McLaughlin, D., Townley, L.R., 1996. A reassessment of the groundwater inverse problem. Water Resour. Res. 32, 1131–1161. https://doi.org/10.1029/96WR00160

Milanovic, P., 2011. Karst Management 47–73. https://doi.org/10.1007/978-94-007-1207-2

Milanovic, P., 2004. Water resources engineering in karst.

Mohammadi, Z., Raeisi, E., Bakalowicz, M., 2007a. Method of leakage study at the karst dam site. A case study: Khersan 3 Dam, Iran. Environ. Geol. 52, 1053–1065. https://doi.org/10.1007/s00254-006-0545-1

Mohammadi, Z., Raeisi, E., Zare, M., 2007b. A dye-tracing test as an aid to studying karst development at an artesian limestone sub-aquifer: Zagros Zone, Iran. Environ. Geol. 52, 587–594. https://doi.org/10.1007/s00254-006-0489-5

Morales-Juberías, T., Olazar, M., Arandes, J., 1997. Application of a solute transport model under variable velocity conditions in a conduit flow aquifer: Olalde karst system, Basque Country, Spain. Springer 30, 143–151.

Morales, T., Angulo, B., Uriarte, J.A., Olazar, M., Arandes, J.M., Antiguedad, I., 2017. Solute transport characterization in karst aquifers by tracer injection tests for a sustainable water resource management. J. Hydrol. 547, 269–279. https://doi.org/10.1016/j.jhydrol.2017.02.009

Mozafari, M., Raeisi, E., Zare, M., 2012. Water leakage paths in the Doosti Dam, Turkmenistan

and Iran. Environ. Earth Sci. 65, 103–117. https://doi.org/10.1007/s12665-011-1069-x

Parise, M., Gunn, J., 2007. Natural and anthropogenic hazards in karst areas: an introduction. Geol. Soc. London, Spec. Publ. 279, 1–3. https://doi.org/10.1144/SP279.1

Pezeshkpoor, P., 1991. Hydrogeological and hydrochemical evaluation of Kuh-e Gar and Barm-Firooz springs. Shiraz university, Iran.

Raeisi, E., 2008. Ground-water storage calculation in karst aquifers with alluvium or no-flow boundaries. J. Cave Karst Stud. 70, 62–70. https://doi.org/PNR61

Raeisi, E., 2002. Carbonate karst caves in Iran.

Raeisi, E., Karami, G., 1997. HYDROCHEMOGRAPHS OF BERGHAN KARST SPRING AS INDICATORS OF AQUIFER CHARACTERISTICS. J. Cave Karst Stud. 59, 112–118.

Rahnemaie, M., 1994. Evaluation of infiltration and runoff in the karstified carbonate rocks. Shiraz University, Iran.

Reimann, T., Geyer, T., Shoemaker, W.B., Liedl, R., Sauter, M., 2011. Effects of dynamically variable saturation and matrix-conduit coupling of flow in karst aquifers. Water Resour. Res. 47, 1–19. https://doi.org/10.1029/2011WR010446

Reimann, T., Giese, M., Geyer, T., Liedl, R., Maréchal, J.C., Shoemaker, W.B., 2014. Representation of water abstraction from a karst conduit with numerical discrete-continuum models. Hydrol. Earth Syst. Sci. 18, 227–241. https://doi.org/10.5194/hess-18-227-2014

Reimann, T., Hill, M.E., 2009. MODFLOW-CFP: A new conduit flow process for MODFLOW-2005.

Ground Water 47, 321–325. https://doi.org/10.1111/j.1745-6584.2009.00561.x

Reimann, T., Liedl, R., Dresden, T.U., Birk, S., Graz, U., Bauer, S., Kiel, U., 2013a. a) First Part – Modifications and Enhancements To Cfpm1 Flow Subroutines a1 . Fixed Head Limited Flow (Fhlq) Boundary Condition.

Reimann, T., Liedl, R., Giese, M., Geyer, T., Maréchal, J.-C., Dörfliger, N., Bauer, S., Birk, S., Shoemaker, W.B., 2013b. Addition and Enhancement of Flow and Transport processes to the MODFLOW-2005 Conduit Flow Process.

Romanov, D., Gabrovšek, F., Dreybrodt, W., 2003. Dam sites in soluble rocks: A model of increasing leakage by dissolutional widening of fractures beneath a dam. Eng. Geol. 70, 17–35. https://doi.org/10.1016/S0013-7952(03)00073-5

Scanlon, B., Mace, R., Barrett, M., Smith, B., 2003. Can we simulate regional groundwater flow in a karst system using equivalent porous media models? Case study, Barton Springs Edwards aquifer, USA. J. Hydrol. 276, 137–158.

Shoemaker, W.B., Cunningham, K.J., Kuniansky, E.L., Dixon, J., 2008a. Effects of turbulence on hydraulic heads and parameter sensitivities in preferential groundwater flow layers. Water Resour. Res. 44. https://doi.org/10.1029/2007WR006601

Shoemaker, W.B., Kuniansky, E.L., Birk, S., Bauer, S., Swain, E.D., 2008b. Documentation of a Conduit Flow Process (CFP) for MODFLOW-2005.

Smart, C.C., Ford, D.C., 1986. Structure and function of a conduit aquifer. Can. J. Earth Sci. 23, 919–929. https://doi.org/10.1139/e86-093

Stöcklin, J., 1971. Stratigraphic Lexicon of Iran. Part I: Central, North and East Iran.

Sudicky, E.A., McLaren, R.G., 1992. The Laplace Transform Galerkin Technique for large-scale simulation of mass transport in discretely fractured porous formations. Water Resour. Res. 28, 499–514. https://doi.org/10.1029/91WR02560

Šumanovac, F., Weisser, M., 2001. Evaluation of resistivity and seismic methods for hydrogeological mapping in karst terrains. J. Appl. Geophys. 47, 13–28. https://doi.org/10.1016/S0926-9851(01)00044-1

Teutsch, G., 1990. An extended double-porosity concept as a practical modelling approach for a karstified terrain. IAHS Publ.

Teutsch, G., Sauter, M., 1998. Distributed parameter modelling approaches in karst-hydrological investigations. Bull Hydrogéol 16, 99–109.

Therrien, R., Sudicky, E.A., 1996. Three-dimensional analysis of variably-saturated flow and solute transport in discretely-fractured porous media. J. Contam. Hydrol. 23, 1–44. https://doi.org/10.1016/0169-7722(95)00088-7

Tolson, B.A., Sharma, V., Swayne., D.A., 2014. Parallel Implementations of the Dynamically Dimensioned Search (DDS) Algorithm. Environ. Softw. Syst. 573.

Tolson, B.A., Shoemaker, C.A., 2008. Efficient prediction uncertainty approximation in the calibration of environmental simulation models. Water Resour. Res. 44, 1–19. https://doi.org/10.1029/2007WR005869

Tolson, B.A., Shoemaker, C.A., 2007. Dynamically dimensioned search algorithm for

computationally efficient watershed model calibration. Water Resour. Res. 43, 1–16. https://doi.org/10.1029/2005WR004723

Wang, X., Jardani, A., Jourde, H., 2017. A hybrid inverse method for hydraulic tomography in fractured and karstic media. J. Hydrol. 551, 29–46. https://doi.org/10.1016/J.JHYDROL.2017.05.051

Weatherill, D., Graf, T., Simmons, C.T., Cook, P.G., Therrien, R., Reynolds, D.A., 2008. Discretizing the Fracture-Matrix Interface to Simulate Solute Transport. Ground Water 46, 606–615. https://doi.org/10.1111/j.1745-6584.2007.00430.x

Welsh, W.D., 2000. GABFLOW: A steady state groundwater flow model of the Great Artesian Basin.

White, W., 1999. Conceptual models for karstic aquifers, in: Palmer, A.N., Palmer, M.V., Sasowsky, I.D. (Eds.), Karst Modeling. Karst Waters Institute Special Publication 5, pp. 11–16.

Winston, R.B., 2009. ModelMuse-A graphical user interface for MODFLOW-2005 and PHAST. Reston, VA.

Worthington, S.R.H., 2015. Diagnostic tests for conceptualizing transport in bedrock aquifers. J. Hydrol. https://doi.org/10.1016/j.jhydrol.2015.08.002

Worthington, S.R.H., 1991. Karst hydrogeology of the Canadian rocky mountains. McMaster University, CANADA.

Xu, Z., Hu, B.X., Davis, H., Cao, J., 2015a. Simulating long term nitrate-N contamination

processes in the Woodville Karst Plain using CFPv2 with UMT3D. J. Hydrol. 524, 72–88. https://doi.org/10.1016/j.jhydrol.2015.02.024

Xu, Z., Hu, B.X., Davis, H., Kish, S., 2015b. Numerical study of groundwater flow cycling controlled by seawater/freshwater interaction in a coastal karst aquifer through conduit network using CFPv2. J. Contam. Hydrol. 182, 131–145. https://doi.org/10.1016/j.jconhyd.2015.09.003

Yen, H., Jeong, J., Smith, D.R., 2016. Evaluation of Dynamically Dimensioned Search Algorithm for Optimizing SWAT by Altering Sampling Distributions and Searching Range. JAWRA J. Am. Water Resour. Assoc. 52, 443–455. https://doi.org/10.1111/1752-1688.12394

Yen, H., Wang, X., Fontane, D.G., Harmel, R.D., Arabi, M., 2014. A framework for propagation of uncertainty contributed by parameterization, input data, model structure, and calibration/validation data in watershed modeling. Environ. Model. Softw. 54, 211–221. https://doi.org/10.1016/j.envsoft.2014.01.004

Zha, Y., Yeh, T.-C.J., Illman, W.A., Tanaka, T., Bruines, P., Onoe, H., Saegusa, H., 2015. What does hydraulic tomography tell us about fractured geological media? A field study and synthetic experiments. J. Hydrol. 531, 17–30. https://doi.org/10.1016/J.JHYDROL.2015.06.013

Zha, Y., Yeh, T.-C.J., Illman, W.A., Tanaka, T., Bruines, P., Onoe, H., Saegusa, H., Mao, D., Takeuchi, S., Wen, J.-C., 2016. An Application of Hydraulic Tomography to a Large-Scale Fractured Granite Site, Mizunami, Japan. Groundwater 54, 793–804. https://doi.org/10.1111/gwat.12421

Zhou, Y., Li, W., 2011. A review of regional groundwater flow modeling. Geosci. Front. 2, 205–214. https://doi.org/10.1016/j.gsf.2011.03.003

Figure captions:

Fig.1: General geological map of the study area showing SLA as the main karst aquifer.

Fig.2: Hydrogeological map of the study area.

Fig. 3: Relationship between the mean annual precipitation and elevation based on adjacent stations. The study area station is shown by a solid rectangle.

Fig. 4: Variation of the river discharge at different gaging stations (IP: Injection Point).

Fig. 5: Flowchart of optimization process using CFPv2 and OSTRICH.

Fig. 6: Geological cross section of the regional groundwater flow and probable paths of the dye movement to the spring.

Fig. 7: Schematic profile (not to scale) along the Maroon River showing the hydrogeological configuration and the assumed scenarios for dye movement.

Fig. 8: The modeling domain and the grid for modeling with CFPv2 in scenarios S0 – S3.

Fig. 9: Variation of objective function versus iteration.

Fig. 10: Values of MRDE (A) and MSE (B) for the spring discharge and the dye concentrations in the different scenarios.

Fig. 11: Plot of the measured versus simulated dye breakthrough curve in each scenario.

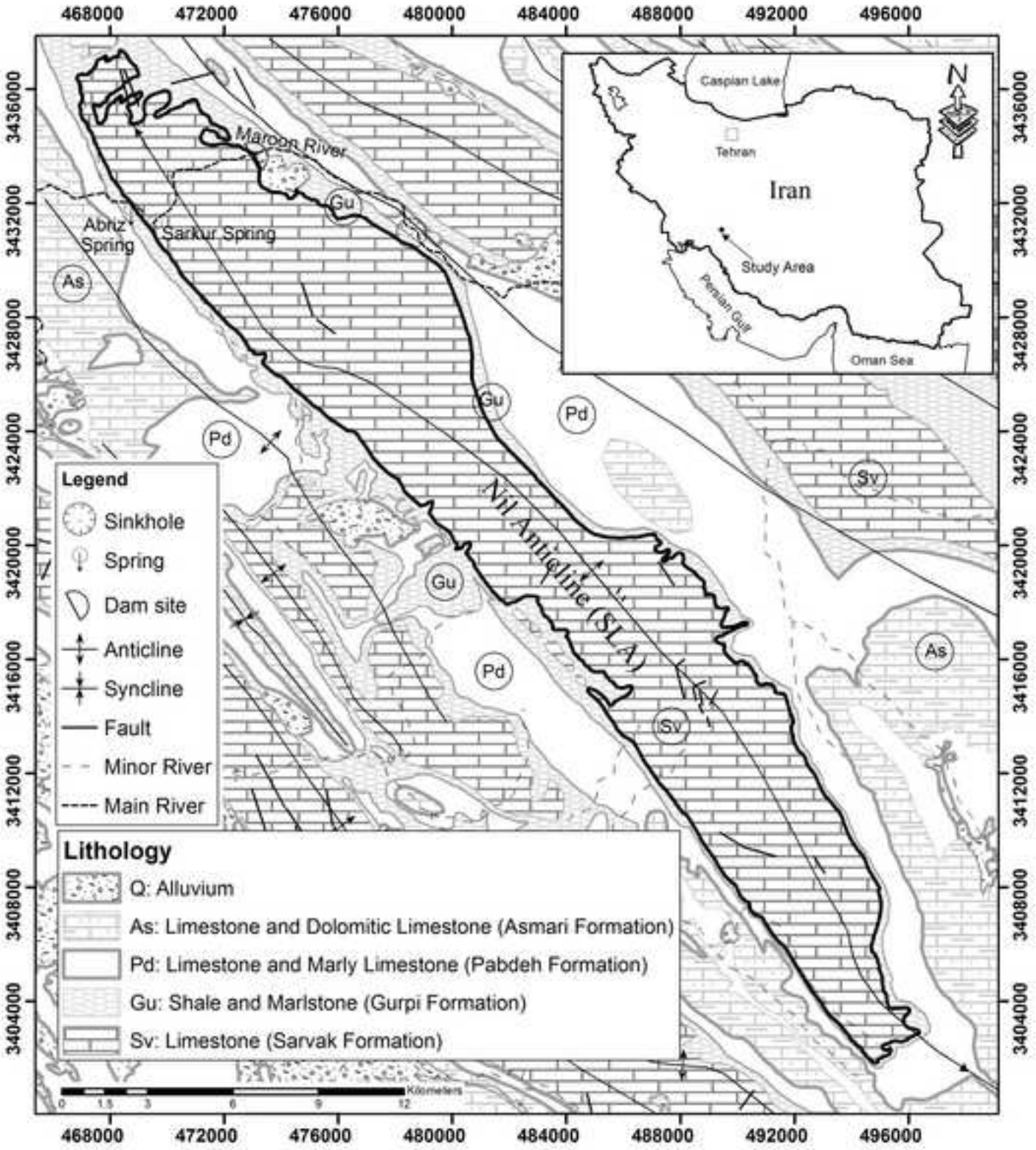

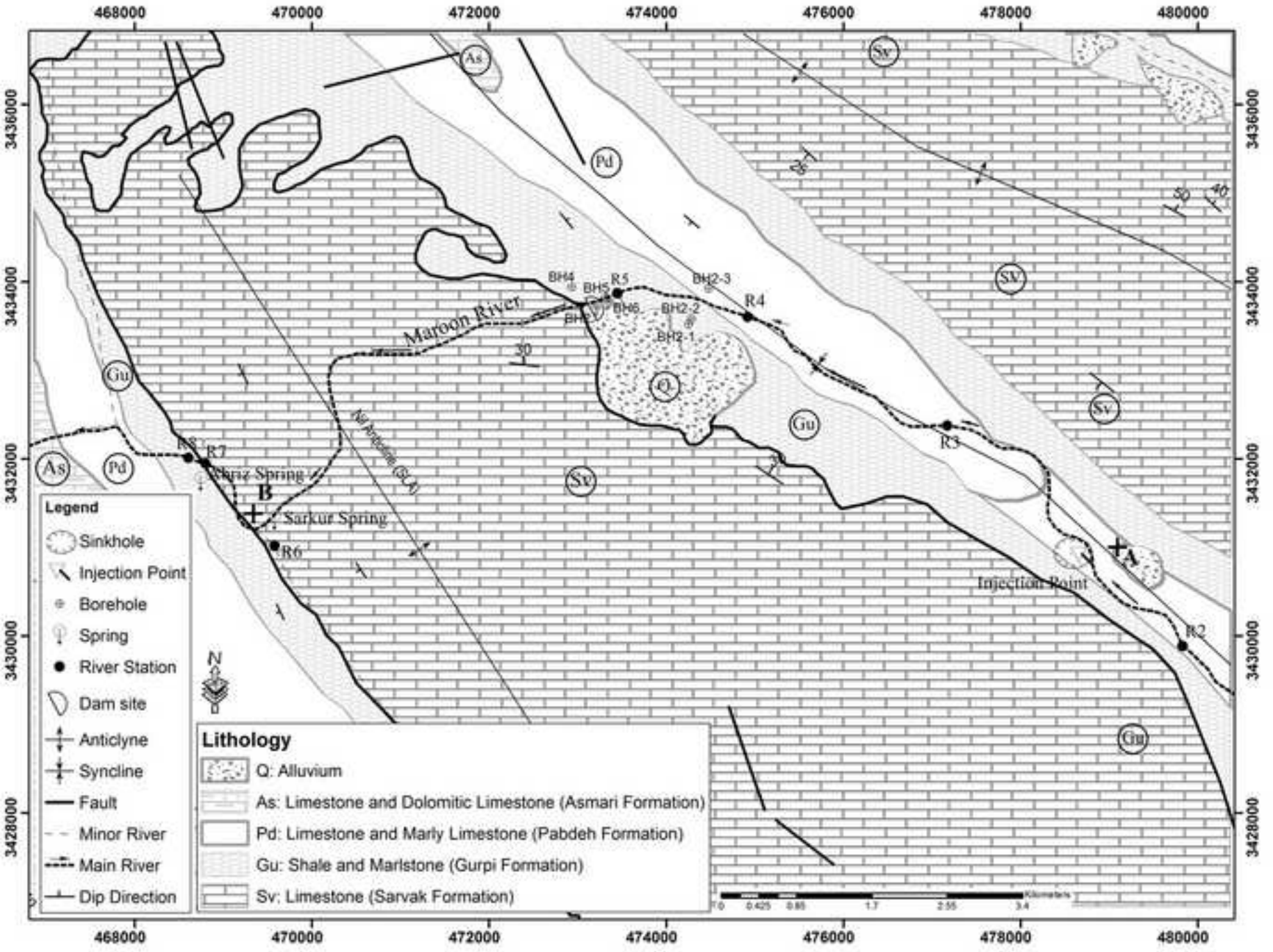

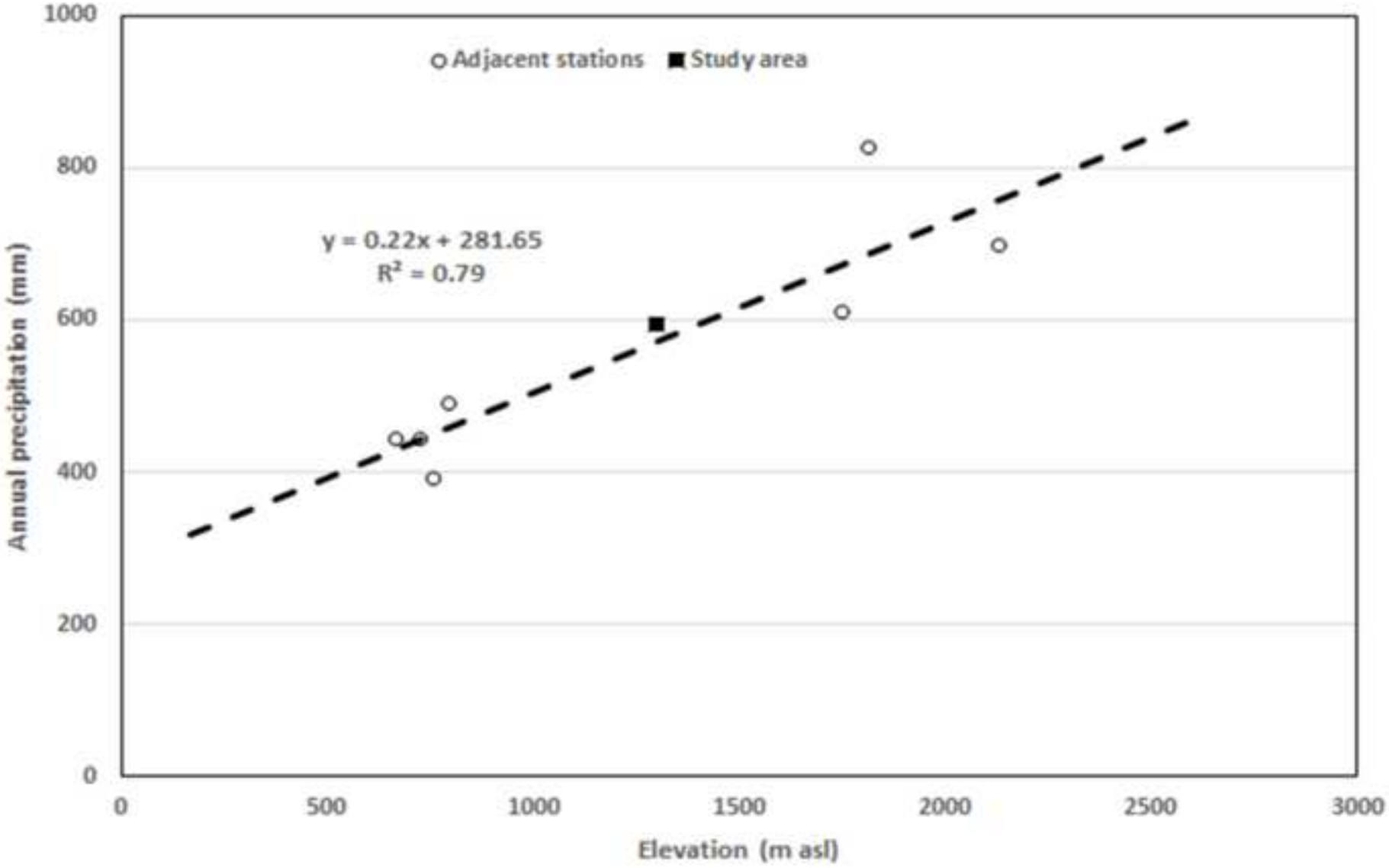

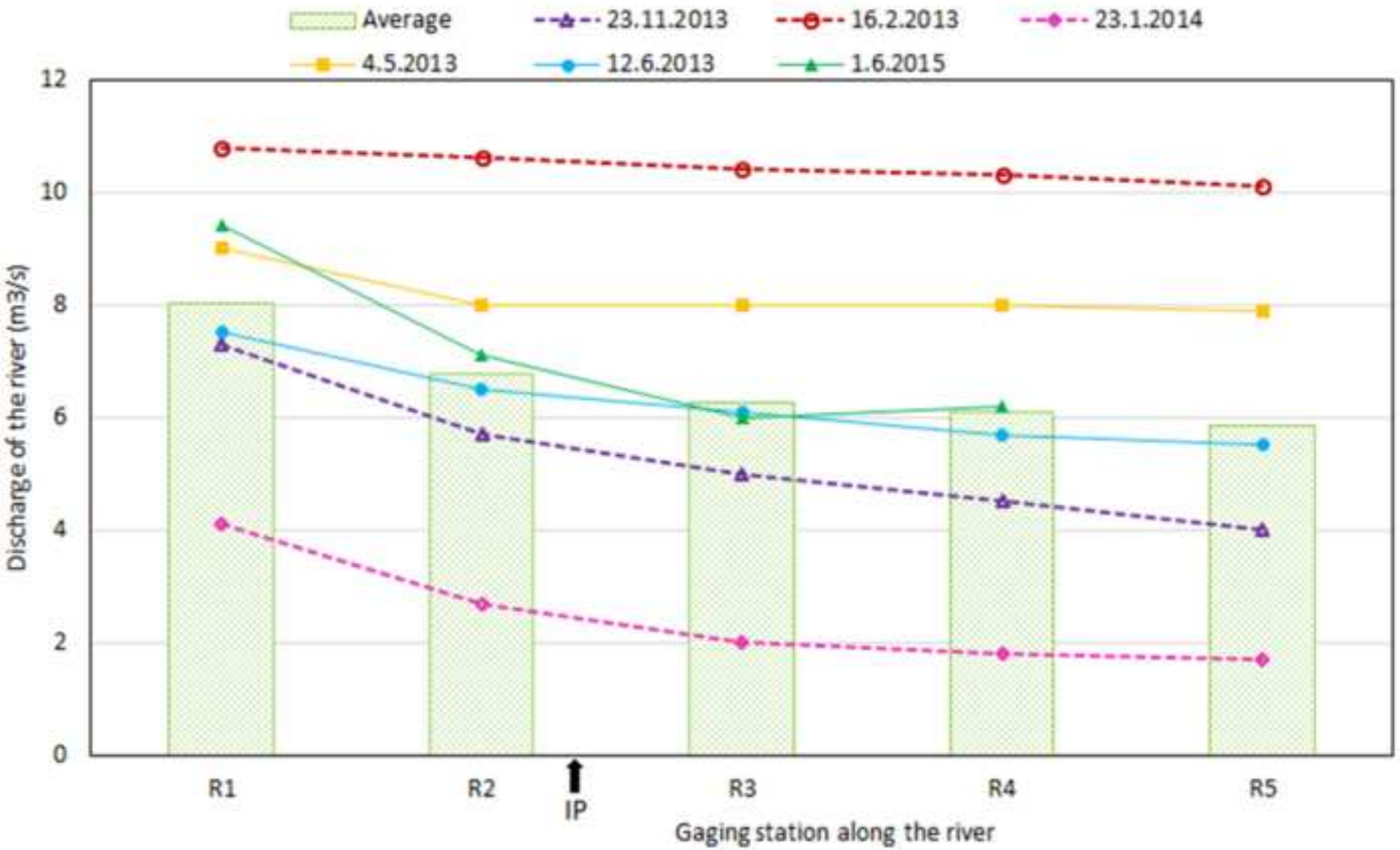

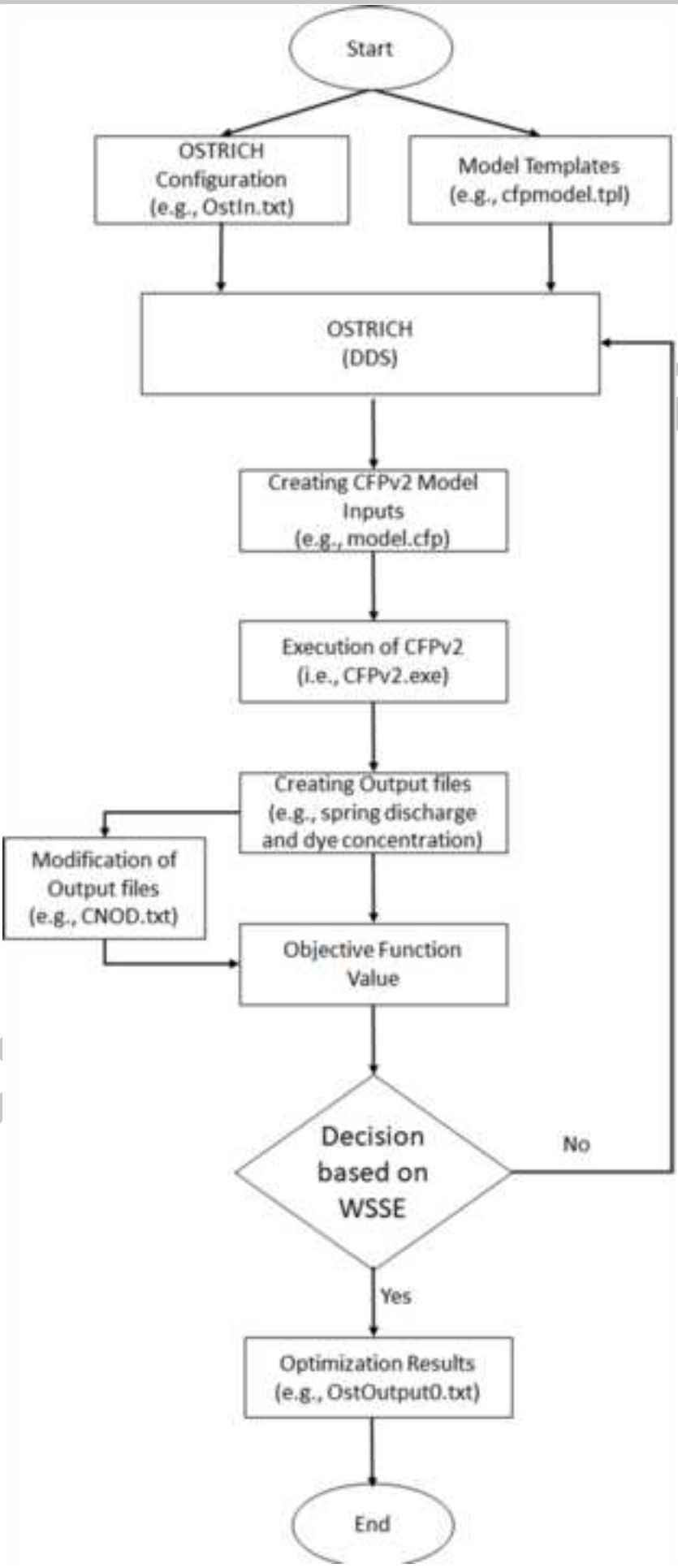

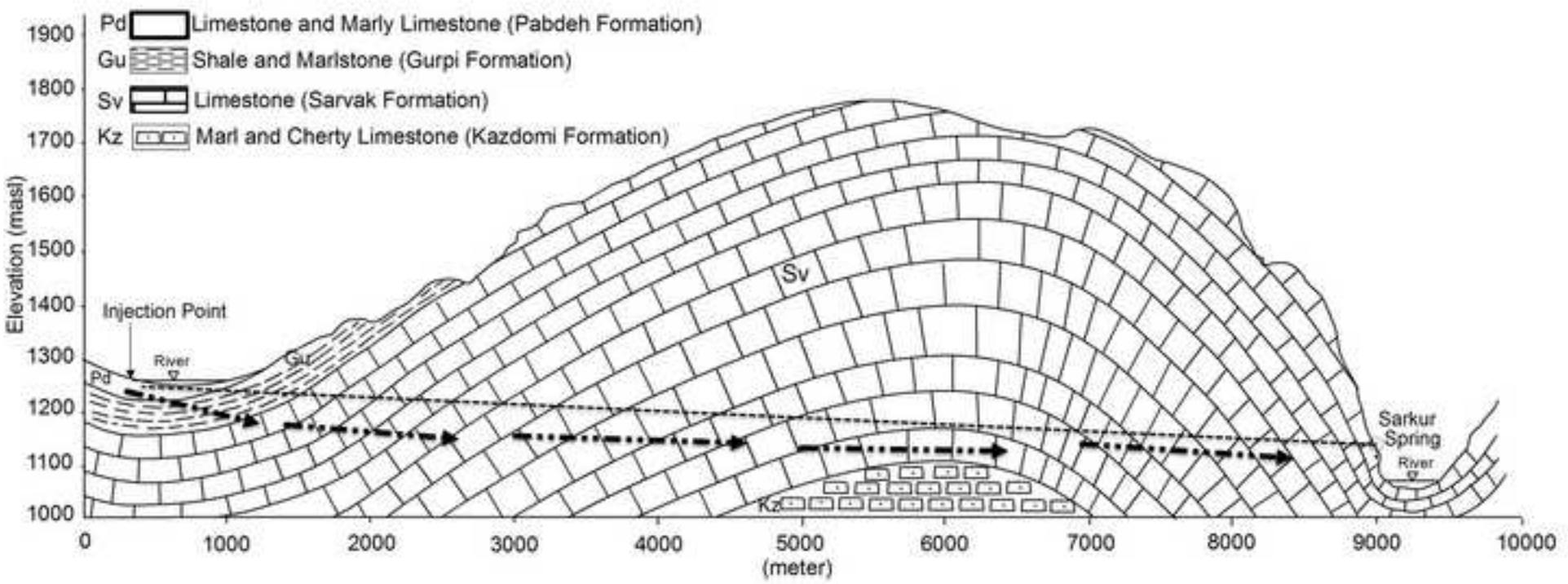

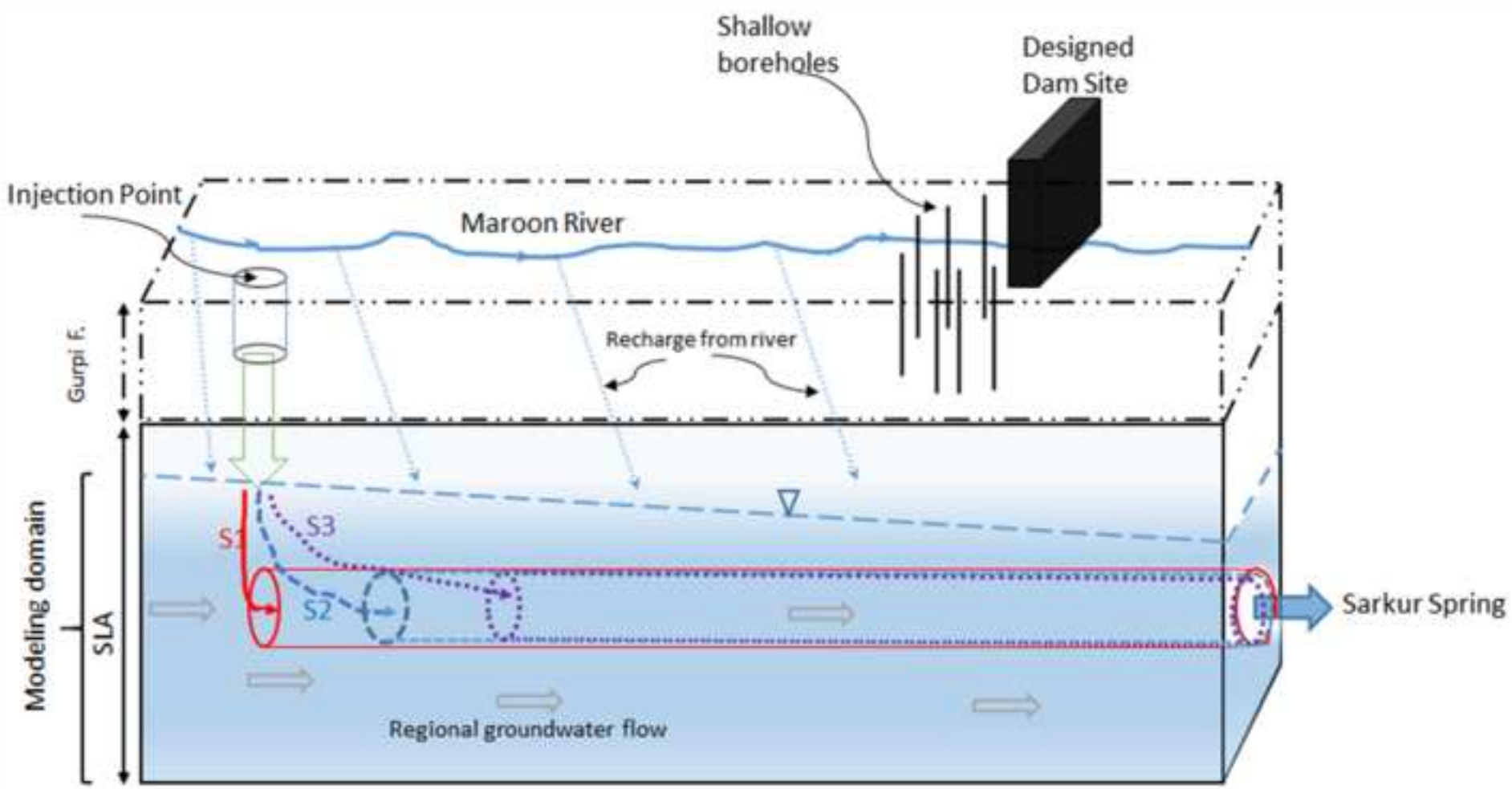

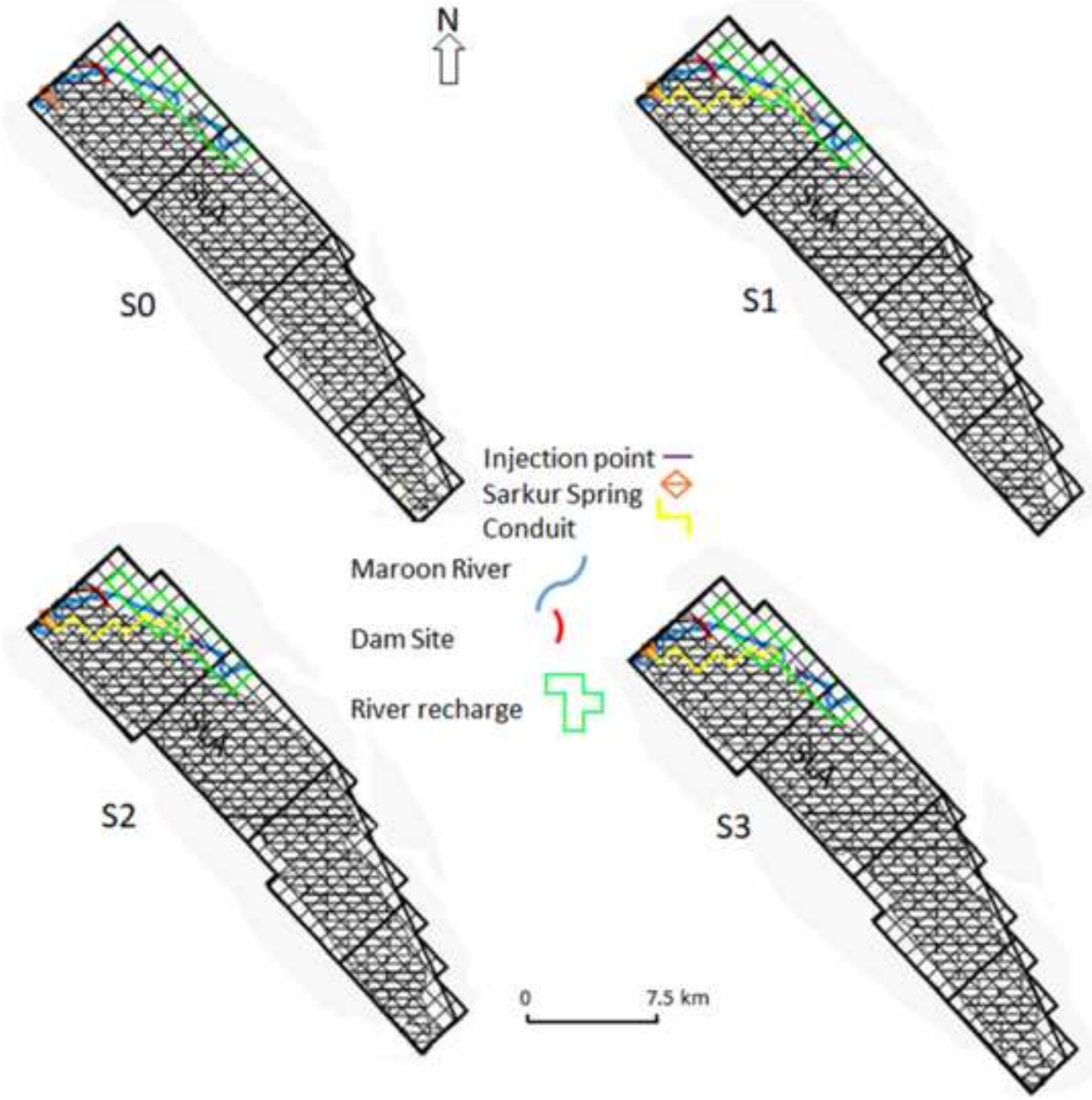

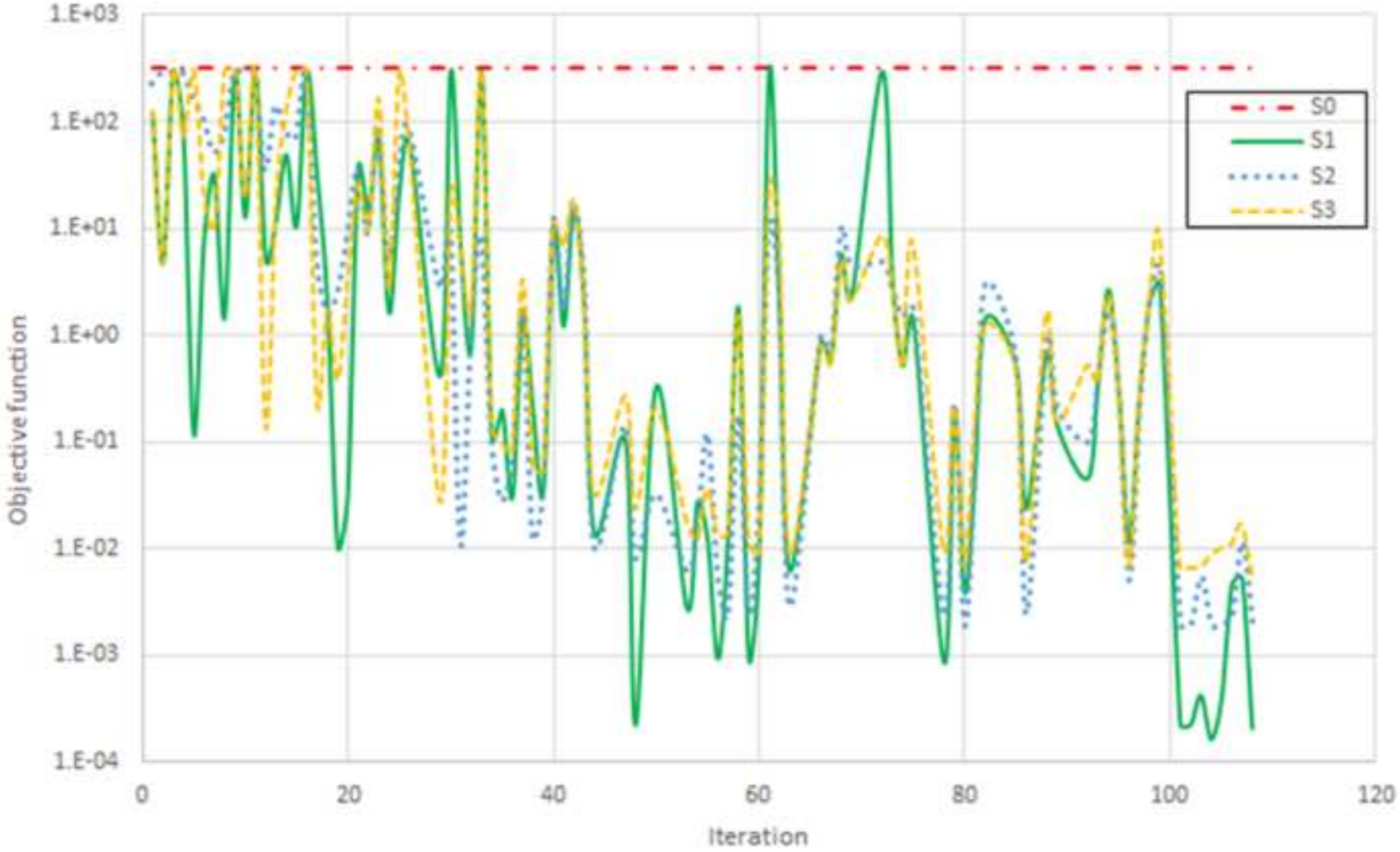

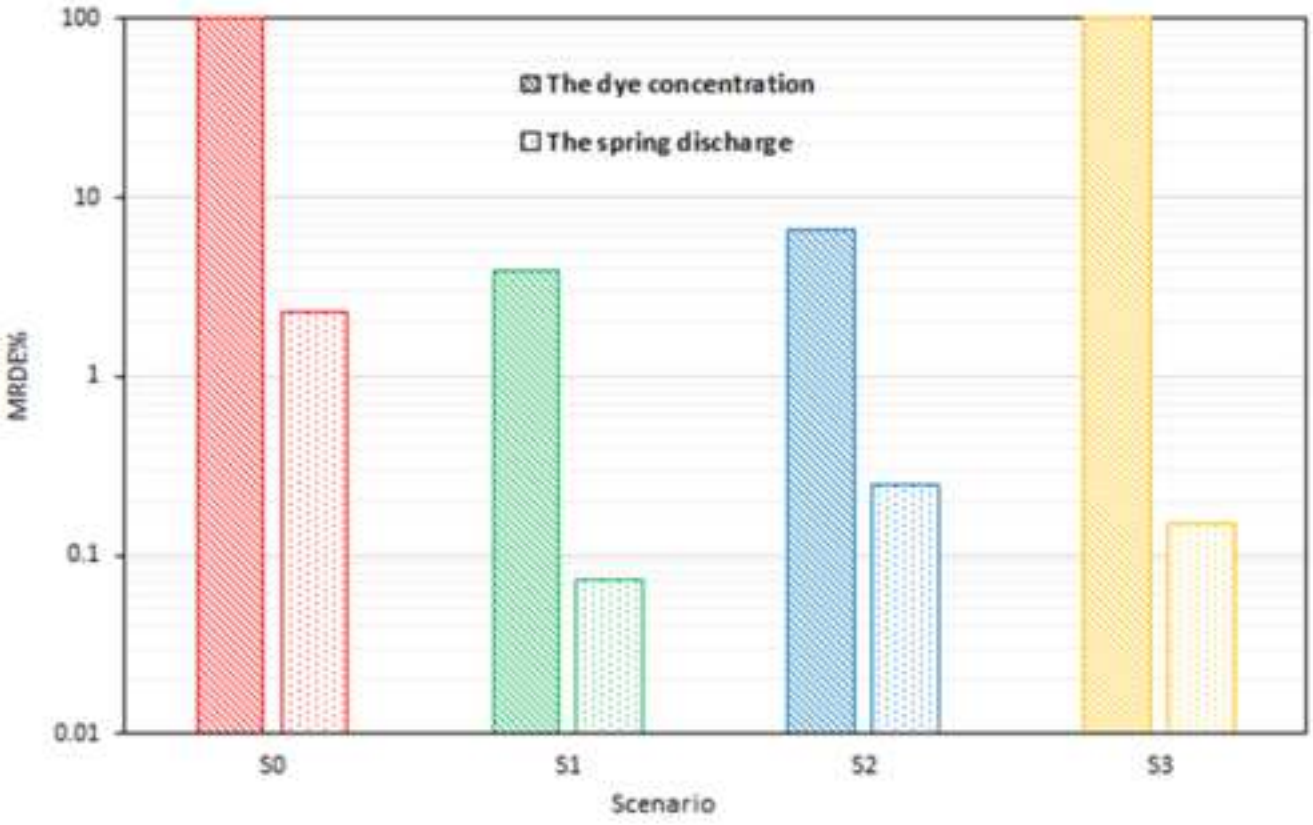

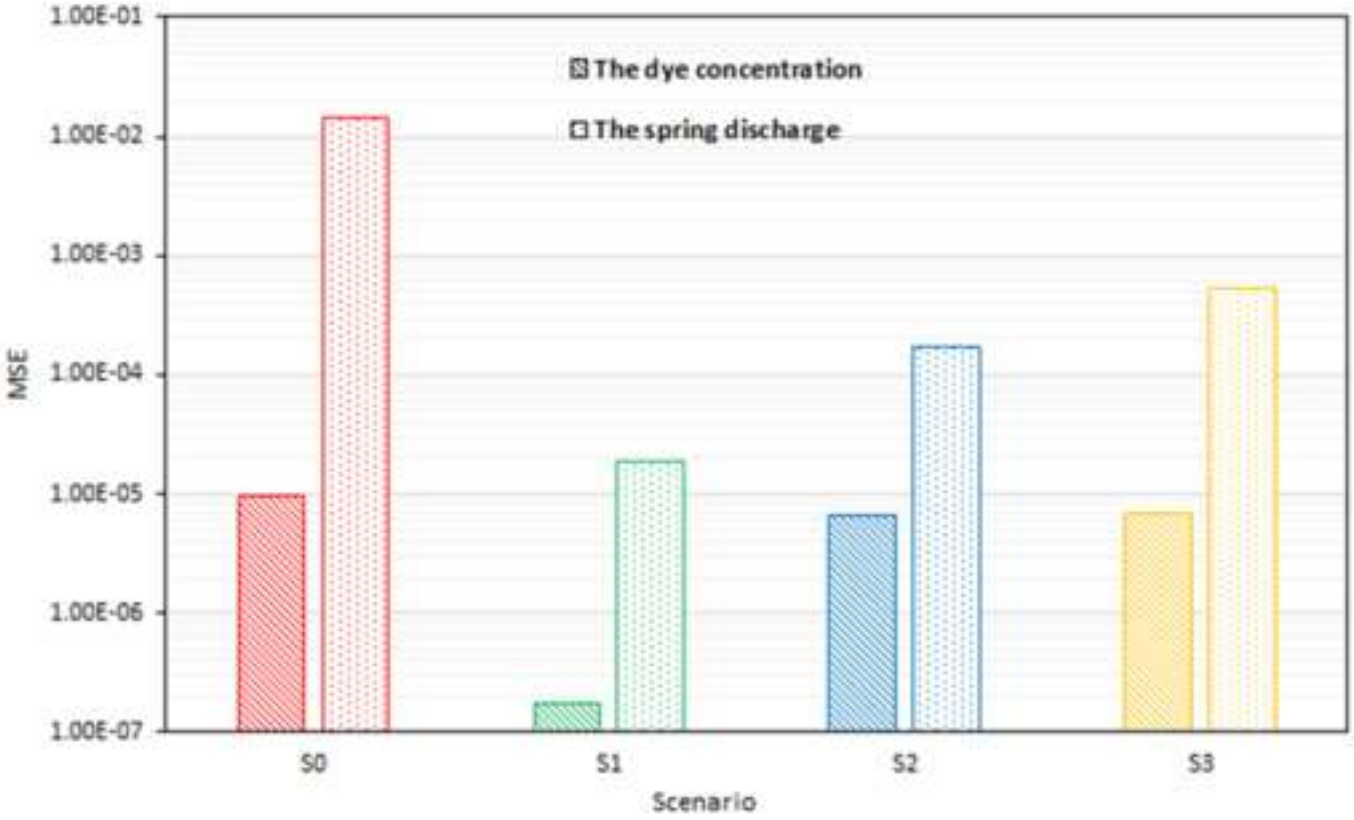

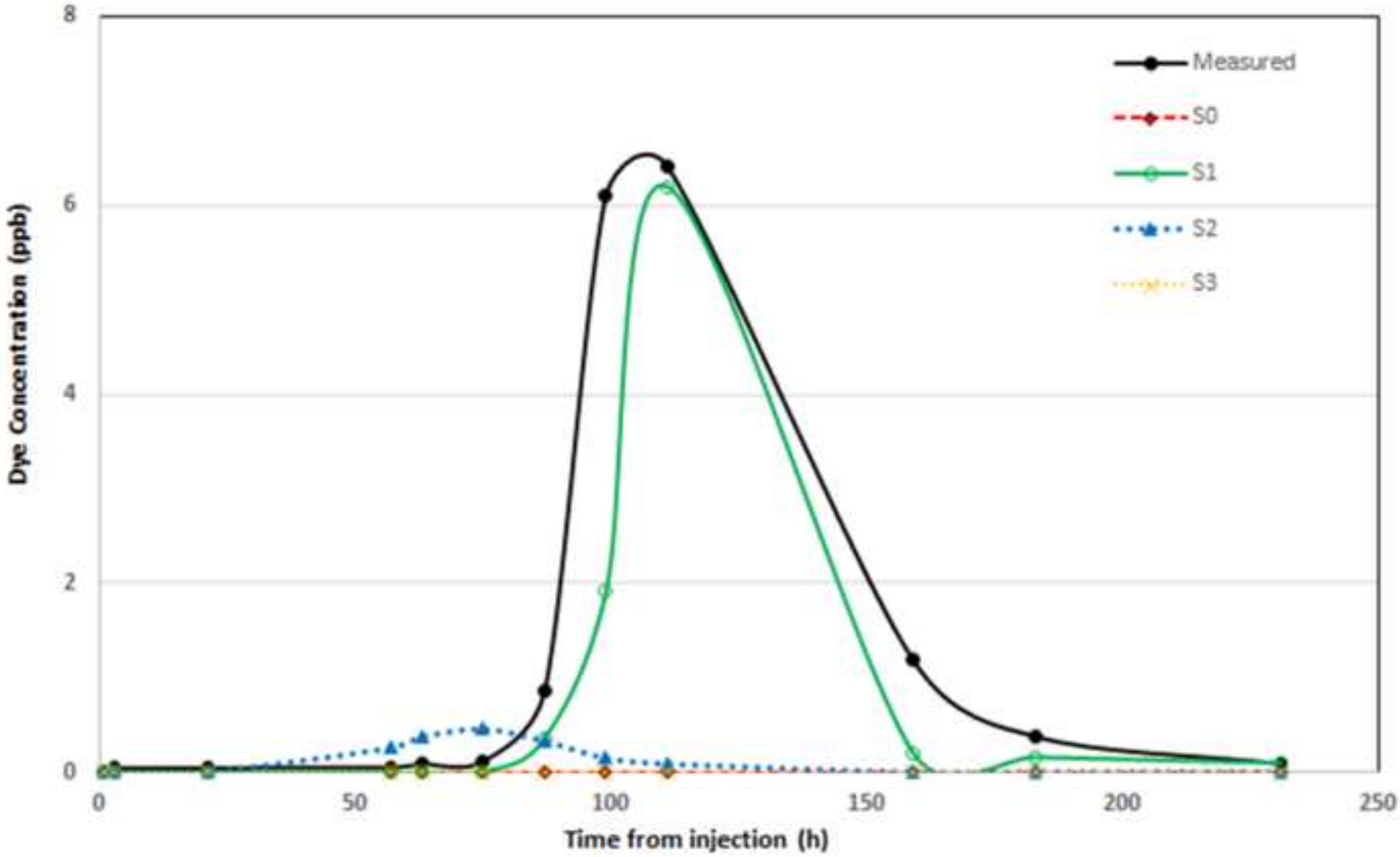

Research highlights:

- First attempt of coupling CFPv2 and OSTRICH for optimization of conduit parameters.
- Calibration of CFPv2 based on considering both breakthrough and spring discharge.
- A reliable scenario is selected that improves understanding of karst groundwater.
- The results contributed to the decision of not constructing a dam at the site.